

THESIS

THE CLIMATOLOGY OF LIGHTNING PRODUCING LARGE IMPULSE CHARGE  
MOMENT CHANGES WITH AN EMPHASIS ON MESOSCALE CONVECTIVE  
SYSTEMS

Submitted by

Nicholas Beavis

Department of Atmospheric Science

In partial fulfillment of the requirements

For the Degree of Master of Science

Colorado State University

Fort Collins, Colorado

Fall 2013

Master's Committee

Advisor: Steven A. Rutledge

Russ S. Schumacher

Walter A. Lyons

Timothy J. Lang

Richard E. Eykholt

## ABSTRACT

### THE CLIMATOLOGY OF LIGHTNING PRODUCING LARGE IMPULSE CHARGE MOMENT CHANGES WITH AN EMPHASIS ON MESOSCALE CONVECTIVE SYSTEMS

The use of both total charge moment change (CMC) and impulse charge moment change (iCMC) magnitudes to assess the potential of a cloud-to-ground (CG) lightning stroke to induce a mesospheric sprite has been well described in literature. However, this work has primarily been carried out on a case study basis. To complement these previous case studies, climatologies of regional, seasonal, and diurnal observations of large-iCMC discharges are presented.

In this study, large-iCMC discharges for thresholds  $> 100$  and  $> 300$  C km in both positive and negative polarities are analyzed on a seasonal basis using density maps of  $2^\circ$  by  $2^\circ$  resolution across the conterminous U.S. using data from the Charge Moment Change Network (CMCN). Also produced were local solar time diurnal distributions in eight different regions covering the lower 48 states as well as the Atlantic Ocean, including the Gulf Stream. In addition, National Lightning Detection Network (NLDN) cloud-to-ground (CG) flash diurnal distributions were included.

The seasonal maps show the predisposition of large positive iCMCs to dominate across the Northern Great Plains, with large negative iCMCs favored in the Southeastern U.S. year-round. During summer, the highest frequency of large positive iCMCs across the Upper Midwest aligns closely with the preferred tracks of nocturnal mesoscale convective systems (MCSs). As iCMC values increase above 300 C km, the

maximum shifts eastward of the 100 C km maximum in the Central Plains. The Southwestern U.S. also experiences significant numbers of large-iCMC discharges in summer, presumably due to convection associated with the North American Monsoon (NAM). The Gulf Stream is active year round, with a bias towards more large positive iCMCs in winter.

Diurnal distributions in the eight regions support these conclusions, with a nocturnal peak in large-iCMC discharges in the Northern Great Plains and Great Lakes, an early- to mid-afternoon peak in the Intermountain West and the Southeastern US, and a morning peak in large-iCMC discharge activity over the Atlantic Ocean. Large negative iCMCs peak earlier in time than large positive iCMCs, attributed to the maturation of large stratiform charge reservoirs after initial convective development.

Results of eight case studies of Northern Great Plains MCSs using the NMQ National Radar Mosaic dataset are also presented. Thresholds described above were used to disseminate iCMC discharges within the MCSs. The radar analysis algorithm on a 5-minute radar volume basis included convective-stratiform partitioning, association of iCMCs and CGs to their respective storms, and statistical analysis on large (100-300 C km) and sprite-class (>300 C km) iCMC-producing storms.

Results from these case studies indicated a strong preference of sprite-class iCMCs to be positive and located in stratiform-identified regions. A 2-3 hour delay in the maximum activity of sprite-class iCMCs after the maximum large iCMC activity was noted, and was strongly correlated with the maximum areal coverage of stratiform area. A loose correlation between more frequent sprite-class iCMC production and larger stratiform areas was noted, suggesting that larger stratiform areas are simply more capable, not more likely, to produce high sprite-class iCMC rates.

Enhanced maximum convective echo heights corresponded to enhanced sprite-class iCMC activity in stratiform areas, attributed in part to enhanced charge advection from the convective line. In situ charging was also presumed to have a significant role in charge generation leading to sprite-class iCMC discharges in stratiform regions.

## ACKNOWLEDGEMENTS

The author would like to thank the NSF for funding support of this work through NSF Grant AGS-1010657.

Many people were involved in the development and completion of this thesis, and due recognition is in order. A very deserved thank you to Steve Rutledge, for invaluable insight and assistance in developing and nurturing ideas presented here, for assistance in becoming a better researcher and member of the scientific community, and for offering the chance to follow a passion that hopefully leads to a career. Thank you to Timothy Lang for all the discussions and helpful tips as well as invaluable help with envisioning the physics of this work (and putting into code). Also thank you to Walt Lyons for productive and engaging discussions of results and helping develop conclusions. Also thanks to committee members Russ Schumacher and Richard Eykholt for their insight and suggestions on how to further improve this work.

The author would also like to extend thanks to the Radar Meteorology Group at Colorado State University for their insights and feedback on material that has gone into this work, in particular Brody Fuchs for fruitful discussions about the physics of the results here and conversion to Python. Especially thank you to Paul Hein, for critical computer and programming assistance. Without him, this work would not have been possible.

The author would also like to extend thanks to fellow students here at Atmospheric Science for their comradery and commiseration with classes and research, Matt and the rest of the footy crew for helping take breaks and listen to rants about how

awesome lightning is, and especially to Kim for helping keep sanity throughout this whole process.

## TABLE OF CONTENTS

|  |      |
|--|------|
| Abstract.....  | ii   |
| Acknowledgements .....   | v    |
| Table of Contents .....  | vii  |
| List of Common Terms and Acronyms .....                                  | viii |
| General Introduction.....  | 1    |
| Section 1: Prepared Manuscript .....                                     | 2    |
| Section 1 Synopsis .....   | 2    |
| Introduction.....  | 3    |
| Data .....   | 6    |
| Methodology .....  | 8    |
| Results: National maps of large-iCMC cloud-to-ground lightning .....     | 10   |
| Results: Regional diurnal distributions of large-iCMC CG lightning ..... | 19   |
| Discussion and Conclusions.....  | 24   |
| Acknowledgements .....   | 31   |
| References .....   | 32   |
| Section 2: Radar Case Studies .....                                      | 41   |
| Section 2 Synopsis .....   | 41   |
| Introduction.....  | 42   |
| Data .....   | 45   |
| Methodology .....  | 46   |
| Results: Overall Statistics .....  | 50   |
| Results: Temporal evolution of variables .....                           | 55   |
| Discussion and Conclusions.....  | 65   |
| References .....   | 73   |
| Overall Conclusions .....  | 82   |

## LIST OF COMMON TERMS AND ACRONYMS

|                   |  |
|-------------------|--|
| CG                | cloud-to-ground lightning flash                                |
| +CG               | positive cloud-to-ground flash                                 |
| -CG               | negative cloud-to-ground flash                                 |
| IC                | Intracloud flash   |
| iCMC              | impulse charge moment change of a CG                           |
| CMC               | charge moment change (total)                                   |
| +iCMC             | positive impulse charge moment change                          |
| -iCMC             | negative impulse charge moment change                          |
| large iCMC        | Section 1: < 100 C km<br>Section 2: 100 C km < iCMC < 300 C km |
| sprite-class iCMC | iCMC < 300 C km  |
| SC iCMC           | sprite-class iCMC  |
| TLE               | transient luminous event                                       |
| MCS               | mesoscale convective system                                    |
| MCC               | mesoscale convective complex                                   |
| CMCN              | Charge Moment Change Network                                   |
| LMA               | Lightning Mapping Array  |
| NLDN              | National Lightning Detection Network                           |
| NMQ               | National Mosaic Quantitative Precipitation Estimation          |
| PAC               | Pacific Coast region   |
| MTN               | Intermountain West region                                      |
| NGP               | Northern Great Plains region                                   |
| SGP               | Southern Great Plains region                                   |
| SEUS              | Southeastern United States region                              |
| LAKE              | Great Lakes region   |
| NE                | New England/Northeastern United States region                  |
| ATL               | Atlantic Ocean region  |
| SA                | surface area   |
| LST               | local solar (overhead) time                                    |
| UTC               | universal coordinated ti                                       |

## GENERAL INTRODUCTION

This study's two main components consist of Section 1, which is a prepared manuscript for submission to *Monthly Weather Review* as well as Section 2, which is more closely related in form to a traditional thesis. The preparation of Section 2 is with an eye towards a conversion into a submitted manuscript, so the structure will be similar to Section 1.

In Section 1, "Regional, Seasonal, and Diurnal Variations of Cloud-to-Ground Lightning with Large Impulse Charge Moment Changes", findings of seasonal, regional, and diurnal trends in large and sprite-class impulse charge moment change (iCMC) activity across the conterminous United States are presented, and the meteorological processes responsible for the results are discussed in a general, macroscopic sense. The findings of this study segue smoothly into Section 2, focusing on large and sprite-class iCMC activity in the Northern Great Plains region, particularly within mesoscale convective systems (MCSs).

In Section 2, eight MCSs producing significant numbers of large and sprite-class iCMCs are analyzed over the course of their lifetimes with national mosaics of radar data. The findings of this portion of the study focus on the evolution of various radar parameters related to the occurrence of large and sprite-class iCMCs primarily in the stratiform region of MCSs. The results of these cases are then generalized, with emphasis on physical processes in the storms.

## SECTION 1

### Regional, Seasonal, and Diurnal Variations of Cloud-to-Ground Lightning with Large Impulse Charge Moment Changes

#### Section 1 Synopsis

The use of both total charge moment change (CMC) and impulse charge moment change (iCMC) magnitudes to assess the potential of a cloud-to-ground (CG) lightning stroke to induce a mesospheric sprite has been well described in literature, on a case study basis. In this climatological study, large-iCMC discharges for thresholds of  $> 100$  and  $> 300$  C km in both positive and negative polarities are analyzed on a seasonal basis in continental density maps. Also presented are local solar time diurnal distributions in eight different regions covering the lower 48 states as well as the Atlantic Ocean, including the Gulf Stream.

The seasonal maps show the predisposition of large positive iCMCs to dominate across the Northern Great Plains, with large negative iCMCs favored in the Southeastern U.S. year-round. During summer, the highest frequency of large positive iCMCs across the Upper Midwest aligns closely with the preferred tracks of nocturnal mesoscale convective systems (MCSs). As iCMC values increase above 300 C km, the maximum shifts eastward of the 100 C km maximum in the Central Plains.

Diurnal distributions in the eight regions support these conclusions, with a nocturnal peak in large-iCMC discharges in the Northern Great Plains and Great Lakes, an early- to mid-afternoon peak in the Intermountain West and the Southeastern US, and a morning peak in large-iCMC discharge activity over the Atlantic Ocean. Large

negative iCMCs peak earlier in time than large positive iCMCs, attributed to the maturation of large stratiform charge reservoirs after initial convective development.

## Introduction

As early as 1925, C.T.R. Wilson predicted atmospheric breakdown high above thunderstorms (Wilson 1925). The topic remained relatively untouched until 1989, with the (re)discovery of sprites- a category of transient luminous events (TLEs) in the mesosphere (Franz et al. 1990). Boccippio et al. (1995) found that sprites were often coincident with highly energetic positive cloud-to-ground (+CG) strokes in the stratiform region of mesoscale convective systems (MCSs) and Schumann resonance excitations. Huang et al. (1999) showed that CGs with large charge moment changes (CMCs) were detectable as Q-bursts, based on Schumann resonance observations in the ionosphere's D-layer. Since then, measurements of charge moment change, the total charge transferred through a vertical lightning channel's length, has been used to predict sprite occurrences and determine their characteristics (Cummer and Inan 2000). This has revealed much about the tropospheric electrical activity linked to mesospheric sprite production. The total CMC of a lightning discharge, particularly positive CGs, is well known to be linked to the production of sprites (Boccippio et al. 1995, Huang et al. 1999, Pasko et al. 2001, Hu et al. 2002, Cummer and Lyons 2005). However, the total CMC is limited in large, continental-scale applications because of the laborious manual hand-fitting of waveforms to produce the CMC for the entire stroke's duration (Lyons and Cummer 2008). As such, the impulse charge moment change (iCMC), representing the

first 2 ms of the total charge moment change (Cummer and Lyons 2004) can effectively be considered to measure the charge moment associated with the return stroke and initial continuing current of a lightning discharge (Rakov and Uman 2003) at continental scales (Hu et al. 2002, Cummer et al. 2013) in real-time (Lyons and Cummer 2008) and therefore provide a clear linkage to sprites.

Recent studies utilizing iCMC have focused primarily on specific cases. Analysis of a mesoscale convective system (MCS) during the Severe Thunderstorm Electrification and Precipitation Study (STEPS) project by Cummer and Lyons (2004) revealed the versatility and importance of iCMC in that it can be measured remotely for a large amount of strokes in large precipitation systems, such as MCSs. Studies such as Cummer and Lyons (2005) further explored iCMC thresholds and the occurrence of sprites over MCSs, which are common over the Great Plains, while more recent studies by Lang et al. (2010, 2011a) analyzed both the iCMC and total CMC over MCSs, highlighting the significance of not only the magnitude of the iCMC, but additional continuing current as well for the initiation of sprites. The propensity of sprite production over MCSs (Boccippio et al. 1995, Lyons 1996) was reinforced by Sao Sabbas et al. (2010) in a study of a prolific sprite-producing MCS over Argentina, where the bulk of the observed sprites occurred over the stratiform precipitation region. Recently, Cummer et al. (2013) produced density maps, identifying preferential regions for large-iCMC (>100 C km) occurrences across the United States, making use of the utility of near real-time capabilities. These regions somewhat match the regions where warm-season MCSs are common (Fritsch et al. 1986). However, no seasonal or diurnal studies of large-iCMC climatologies have been presented to date.

A typical CG stroke has an average charge of 20 C lowered to ground over an average channel length of 7.5 km over 300 ms (Rakov and Uman 2003). Such common strokes would have an iCMC of less than 10 C km. The theoretical minimum on sprite initiation from total CMC data has been reported to be 200 C km (Qin et al 2012), although sprites have been observed from CGs with CMCs as low as 120 C km (Hu et al 2002). Thus, the type of lightning analyzed in this study is as Williams et al. (2012) termed as “exceptional” or “superlative” lightning that can loudly “ring” the Earth-ionosphere cavity. Such powerful (and especially long continuing-current) strokes are important to many engineering aspects, such as aviation and construction. The amount of charge transferred to ground by a CG is not easily retrievable, in part due to only the peak current being measured by the NLDN (as opposed to continuing current). However, the total charge associated with a CG can be obtained if lightning mapping array (LMA) data are present (Lyons et al. 2003, Lang et al. 2010, Lang et al. 2011b). As seen above, iCMC strokes have order of magnitude larger iCMCs than garden-variety CGs, then the charge transferred to ground would also be presumed to be at least an order of magnitude larger. Strokes with high charge transfer could be damaging to aircraft and electrical systems, as well as have a higher propensity for starting fires (e.g. wildfires, structure fires; Curran et al. 2000). Additionally, upward-triggered lightning from tall objects (e.g. towers) has been noted to coincide with large-iCMC discharges (Warner 2011, Warner et al. 2012a, 2012b).

Observations in Cummer et al. 2013 of the lack of a monotonic increase in iCMC with increasing peak current suggest that a significant continuing current on a relatively modest iCMC could transfer enough charge to initiate a sprite, echoing the observations of sprite initiation from long continuing currents (up to 150 ms; Cummer and Fullekrug

2001). In addition to climatologies of large iCMCs, comparison with NLDN climatologies can reveal the behavior of large-iCMC strokes in relation to “normal” CG strokes. Diurnal and seasonal distributions for regions covering the entire contiguous United States as well as national seasonal maps have been prepared, in an effort to better understand the behavior of large iCMCs on long temporal scales. Distributions of iCMCs >100 C km (similar to Cummer et al. 2013) and larger iCMCs > 300 C km will help to understand the climatology of sprites, as well as their spatial and temporal distribution on a variety of scales.

## Data

This study utilizes of two main data components: real-time iCMC estimates from the national Charge Moment Change Network (CMCN) as well as flash data from the NLDN.

### *a. Charge Moment Change Network*

The CMCN is comprised of two stations: one near Duke University in Durham, NC at 35.975°N, 79.100°W and the other at Yucca Ridge Field Station (YRFS), outside Fort Collins, CO at 40.668°N, 104.937°W (Lyons and Cummer 2008, Cummer et al. 2013). The iCMC is diagnosed from extremely low frequency (ELF) magnetic field observations, using linear regularization techniques developed by Cummer and Inan (2000) to extract the charge moment waveform. NLDN data are used for geolocation of the parent flash and quality control (Cummer and Inan 2000). As mentioned by Cummer et al (2013), NLDN-detected events with peak currents less than 10 kA are not

processed for iCMCs due to the high number of events of this type. The iCMC values can be reliably measured some 2000 km from either station (Hu et al. 2002, Cummer and Lyons 2004), such that the network covers the entire conterminous United States, shown in Fig. 1. In the case of duplicate detections in the overlapping region, the Duke sensor is given preference due to less noise at that sensor (Lyons and Cummer 2008, Cummer et al. 2013). Other limitations and network performance of the iCMC dataset are described in detail by Lyons and Cummer (2008) and Cummer et al. (2013). The processed iCMC dataset used by this study extends continuously from 1 August 2007 to 31 July 2012, for 5 complete years of data. A near real-time iCMC internet display, updated every 5 minutes, has been routinely monitored since 2007. This display has been used successfully in orienting cameras to capture sprites during observation campaigns.

#### *b. National Lightning Detection Network*

NLDN flash-level data spanning the same time period were also used in this study. Contained within the NLDN data are geolocation, time, peak current, an intracloud (IC) or CG flag, as well as other parameters such as multiplicity (Cummins et al 1998a). The description and system performance of the NLDN following the installment of a time-of-arrival locating feature is detailed by Cummins et al. (1998a). Recent upgrades, including the criteria for classifying CG events being any CG-flagged flash with peak current magnitude larger than 15 kA (classifying those below this threshold as ICs; Murphy and Cummins 2009), or an intracloud-identified flash with peak current magnitude larger than 25 kA (K. Cummins 2013, personal communication). If the NLDN fails to detect a CG, then the accompanying iCMC will not be entered into the

database. Approximately 10% of sprite-class +CGs are not processed in real-time (W. Lyons 2013, personal communication). Thus, the estimates of the large iCMC population in this study are slightly lower than in reality. These criteria are applied in this study to identify CG flashes in the domains shown in Fig. 1.

## Methodology

The diurnal and seasonal climatology of large-iCMC and NLDN events focused on regions identified based on surface topographical differences as well as lightning differences. Figure 1 shows the regional boxes used. Beginning in the west, the Pacific Coast (PAC) region was meant to capture mostly isolated large-iCMC events associated with cold-season extratropical cyclones making landfall along the U.S. West Coast (Lyons et al 2012; Orville and Huffines 2011) and isolated, primarily terrain-driven warm-season convection. The Intermountain West (MTN) domain was meant to capture most of the Rocky Mountain cordillera along with the isolated, terrain-induced convection common in summer months, often associated with the North American Monsoon (Badan-Dangon et al. 1991). Because the Rocky Mountains curve westward in the northern reaches of the domain, some storms more characteristic of the Northern Great Plains may be captured as well. The southern border of the Northern Great Plains (NGP) domain was placed in the middle of Kansas to capture the observed maximum in positive CG (+CG) percentage extending from western Kansas north-northeastward to southern Manitoba (Lyons et al. 1998, Zajac and Rutledge 2001, Orville et al 2011). The NGP region has also contributed to the bulk of known optical sprite observations (Lyons 1996, Lyons et al. 2003, 2006, 2009). The Great Lakes (LAKE) region was

selected to contain the Great Lakes, which can modulate summer convection significantly, including mesoscale squall lines (Lyons 1966, Nicholson and Yin 2002). The Southern Great Plains (SGP) has NGP as a northern boundary, and the eastern boundary for SGP was chosen to exclude the topography associated with the Ozark Mountains. The Southeastern US (SEUS) was the remainder of the U.S. south and east of the SGP and LAKE regions, containing much of the high-multiplicity -CG lightning observed over the United States (Orville et al 2011). Convection over the Gulf Stream produces enough lightning (Hobbs 1987, Orville 1990) to warrant its own region, and thus the Atlantic Ocean (ATL) domain is meant to contain as much of the Gulf Stream in its domain as possible. The Northeast (NE) domain contains the remainder of the conterminous US for completeness.

Since both iCMC and additional continuing current contribute to the total charge moment change, an iCMC of 100 C km is adjudged to be an adequate lower limit for “large” iCMCs (following Cummer et al. 2013). However, a fixed lower threshold on CMC (and iCMC) is unlikely, but rather a range of CMC over which the probability of sprite initiation increases from minimal to highly likely (Hu et al. 2002). Lightning events were considered “sprite-class” if their iCMCs were above 300 C km, owing to a 75-80% probability of sprite initiation from a +CG (Cummer and Lyons 2005; Lyons et al. 2009). The 300 C km threshold is also the theoretical minimum threshold for a -CG to produce a sprite (Qin et al. 2012).

Within each region, large iCMC events  $> 100$  C km and sprite-class iCMCs  $> 300$  C km were sorted into hourly (local solar time) bins to produce a diurnal distribution. The local solar time for iCMC event can be computed by extracting the observed UTC time

from the CMCN and adjusting for the longitude of each observation. The NLDN CG events also were sorted in the same manner in each region.

## Results

### *a. National maps of large-iCMC cloud-to-ground lightning*

Cummer et al. (2013) presented three-year national stroke density maps for large iCMC CG lightning strokes ( $\geq 100$  C km) in the United States and surrounding areas. In the present analysis, this has been extended to five years (August 2007 through July 2012). The 5-year stroke density maps ( $2^\circ$  latitude/longitude resolution) for iCMC values greater than 100 C km are shown in Fig. 2a and 2b. For the positive (Fig. 2a) strokes (559,562 total for the 5 years), the results are fundamentally similar to the 3-year climatology shown in Cummer et al. (2013; their Fig. 12). The positive maximum remains in central Nebraska, with secondary maxima centered on western Tennessee (plus portions of surrounding states) and over the Gulf Stream. These are geographically offset from the negative maximum (Fig. 2b; 403,802 strokes total for the 5 years), which occurs over the Gulf Coast (eastern Louisiana through western Florida). However, the Gulf Stream remains active for large-iCMC negatives in addition to positives. Cummer et al. (2013) did not present a corresponding map for  $-100$  C km strokes.

The 5-year climatologies were broken down by season for positive (Fig. 3) and negative (Fig. 4) strokes with iCMC  $> 100$  C km. In order to improve dynamic range in these plots, the stroke totals have been annualized based on the amounts during each season, and thus densities can be larger than the values shown in Fig. 2. In the winter

(Fig. 3a), large positive iCMCs mainly occurred over the southeastern United States - specifically, Alabama, Mississippi, and Tennessee. There is another small maximum over the Gulf Stream. Large positive iCMC stroke densities increase and move northward and westward in the spring (Fig. 3b). At this point there are two separate maxima - one again focused on western Tennessee similar to the overall climatology (Fig. 2a), and another broadly centered over the Kansas/Oklahoma border region. Gulf Stream activity grows in magnitude and extent during this season. In summer (Fig. 3c), activity again continues its northward and westward march, and there is a very strong maximum over central Nebraska, which is clearly the cause of the same maximum seen in the overall climatology (Fig. 2a). Significant large iCMC activity (at least  $10^{-2} \text{ km}^{-2} \text{ yr}^{-1}$  annualized stroke density) reaches its greatest spatial extent during summer, including increased activity in northwestern Mexico, evidently associated with the North American Monsoon (Adams and Comrie 1997). The Gulf Stream continues to be active as well. Large positive iCMCs decrease rapidly in the fall (Fig. 3d), and the maximum remains in the Central Plains states, while a secondary maximum continues to occur over the Gulf Stream.

In the winter (Fig. 4a), large negative iCMCs are displaced southwestward of the positive maximum, although the negatives remain in the southeastern United States, especially Louisiana and southern Mississippi. This maximum increases in density during the spring (Fig. 4b), while activity also spreads northwestward to form a secondary maximum over Arkansas, and activity over the Gulf Stream develops. Maximum spatial coverage occurs in summer (Fig. 4c), similar to large positive iCMCs (Fig. 3c), but again there is a notable regional offset. Large negative iCMCs continue to dominate in the Southeast, even as the overall activity spreads northwestward into the

Central Plains and the desert Southwest/northwestern Mexico. There is a secondary maximum in the Central Plains, but it is displaced eastward from the positive maximum. The Gulf Stream is significantly more active for negatives in summer than spring. Finally, during autumn months, (Fig. 4d) activity declines appreciably, although, the Southeast and the Gulf Stream continue to see a broad maximum in large negative iCMCs. In addition, a secondary maximum of negatives continues to be produced over the Central Plains, interestingly in roughly the same location as the positive maximum during this time period (Fig. 3d).

To examine the sensitivity of these large-iCMC climatologies to the choice of threshold, and to look for interesting differences that may reflect the influence of precipitation system evolution, the basic  $>300$  C km climatologies are shown in Fig. 2c and 2d. Despite the approximate factor of 10 reduction in stroke density by moving to the higher threshold (74,585 positive strokes over the 5-year period, and 15,140 negative strokes), the  $>300$  C km climatologies are fundamentally similar to the  $>100$  C km climatologies. One notable difference, however, is that the positive maximum in the Central Plains (Fig. 2c) is displaced slightly eastward of the  $>100$  C km. This was also seen in the 3-year climatology presented in Cummer et al. (2013).

The western Tennessee secondary maximum is not displaced, though, and neither is the negative maximum, which remains over southern Louisiana and Mississippi. Another interesting difference is that the Gulf Stream is a much larger producer of  $>300$  C km positives relative to  $>300$  C km negatives, whereas for  $>100$  C km strokes the production was more equal. This probably reflects the fact that very few -CGs produce extremely high iCMC values like 300 C km, compared to +CGs (Cummer et al. 2013).

The seasonal variability of  $>300$  C km +CGs (Fig. 5) also is fundamentally similar to the  $>100$  C km +CGs, but the eastward displacement of the  $>300$  C km maximum in the Central Plains (particularly into Iowa) is most prevalent during summer (Fig. 5c). The seasonal variability of  $>300$  C km -CGs (Fig. 6) is very similar to the  $>100$  C km strokes, though again there is a much greater relative reduction for negative strokes at this higher threshold than there is for positive strokes (Cummer et al. 2013).

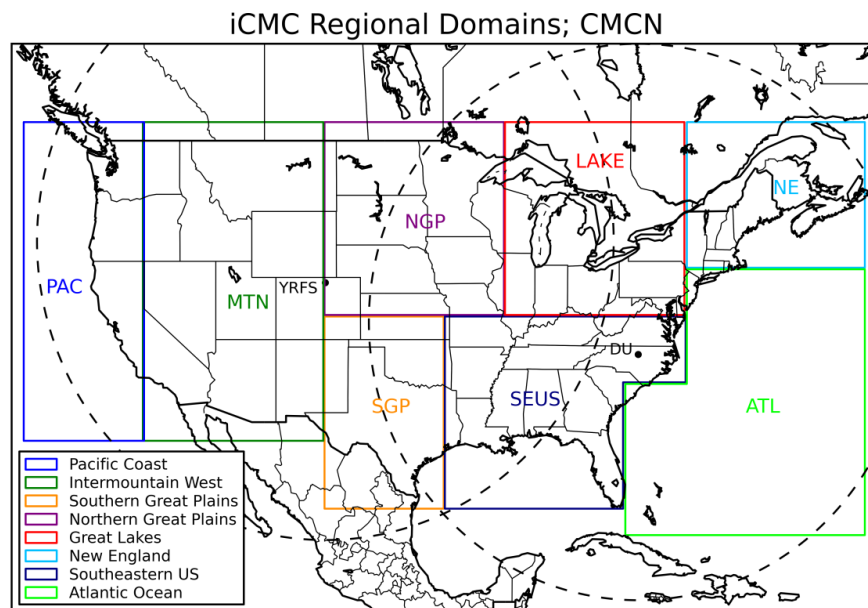


**Figure 1.** Regional domains used in the analysis of iCMC and NLDN diurnal and seasonal climatologies. The short descriptors are as follows: Southern Great Plains (SGP), Northern Great Plains (NGP), Southeastern US (SEUS), Great Lakes (LAKE), New England (NE), Atlantic Ocean (ATL), Intermountain West (MTN), and Pacific Coast (PAC). Also shown on the map is the coverage of the CMCN (dashed black line) as well as the location of the CMCN sensors at YRFS and DU (black dots).

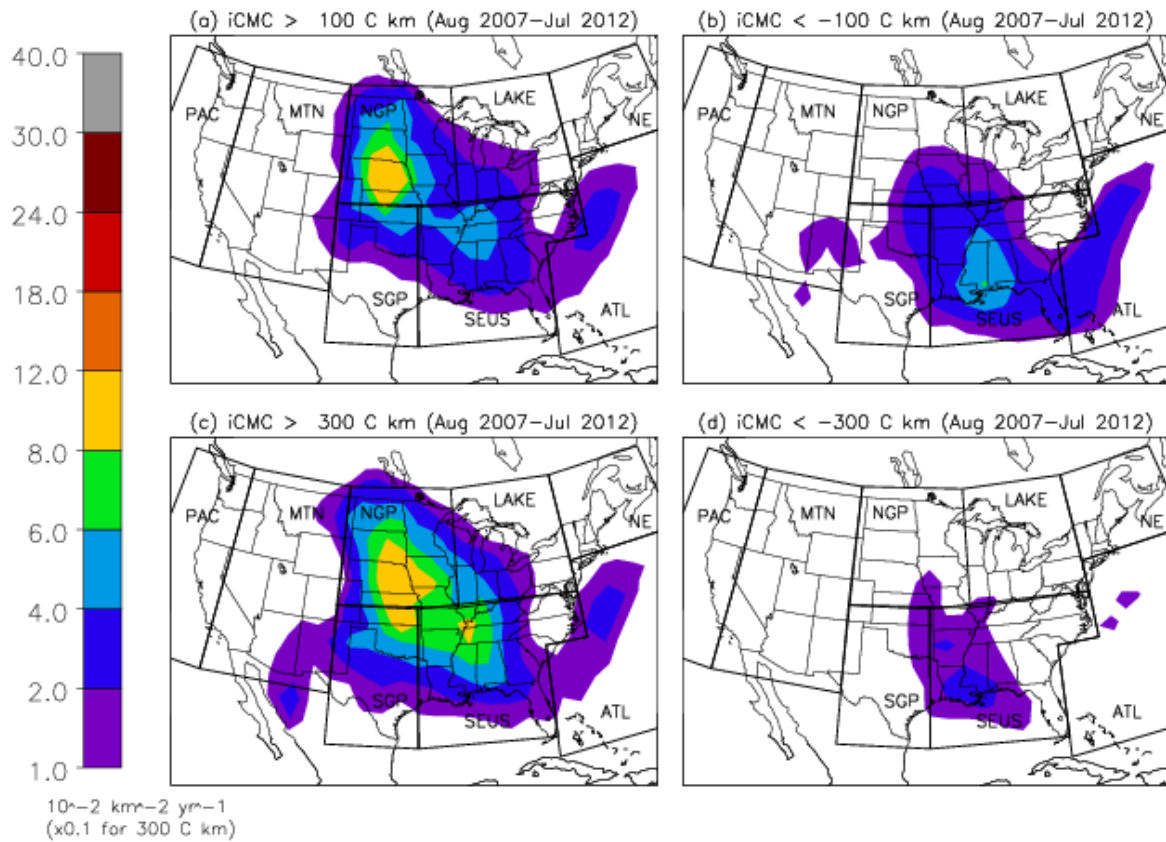


**Figure 2.** Density maps for strokes with iCMC values greater than 100 C km, for August 2007 through July 2012. (a) Positive strokes. (b) Negative strokes; Density maps for strokes with iCMC values greater than 300 C km, for August 2007 through July 2012. (c) Positive strokes. (d) Negative strokes. Note that the two bottom panels for the >300 C km maps are multiplied by 0.1 of the scale for >100 C km strokes.

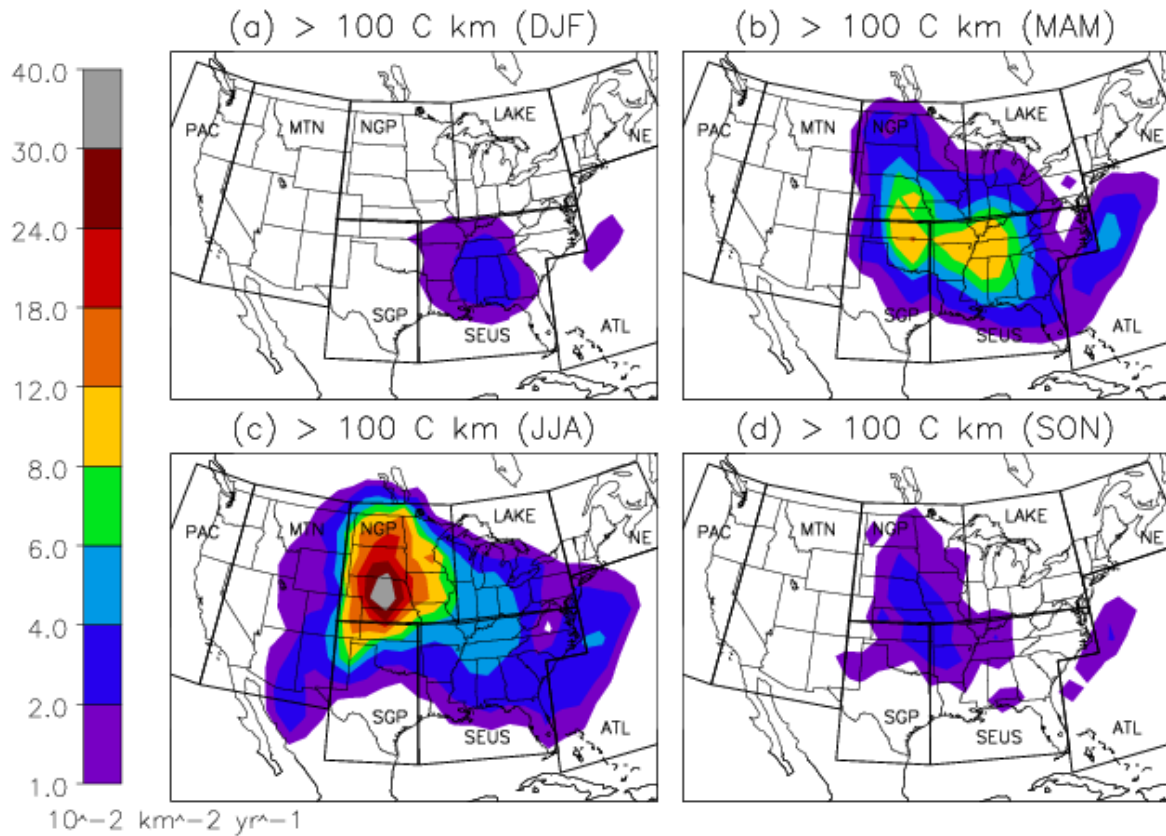


**Figure 3.** Annualized density maps for positive strokes with iCMC values greater than 100 C km, broken down by season for the period August 2007 through July 2012. (a) December through February (Winter). (b) March through May (Spring). (c) June through August (Summer). (d) September through November (Fall).

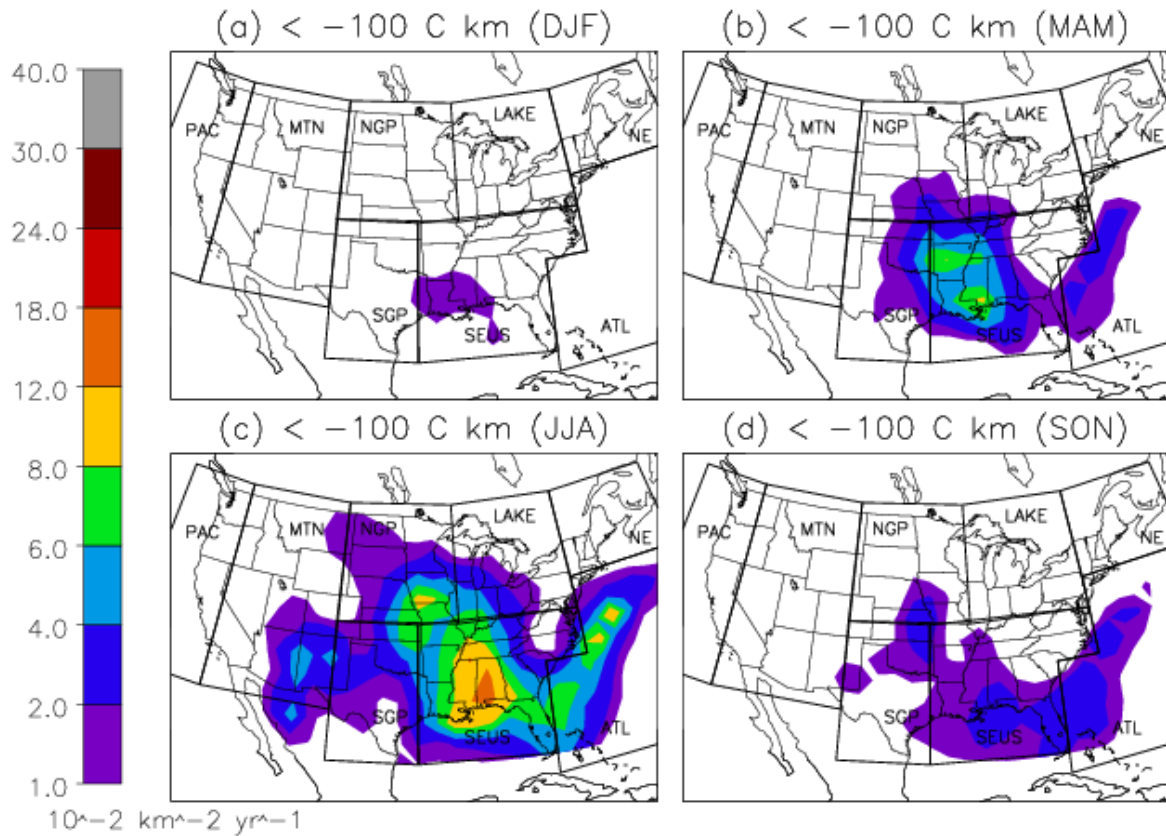


**Figure 4.** Annualized density maps for negative strokes with iCMC values greater than 100 C km, broken down by season for the period August 2007 through July 2012. (a) December through February (Winter). (b) March through May (Spring). (c) June through August (Summer). (d) September through November (Fall).

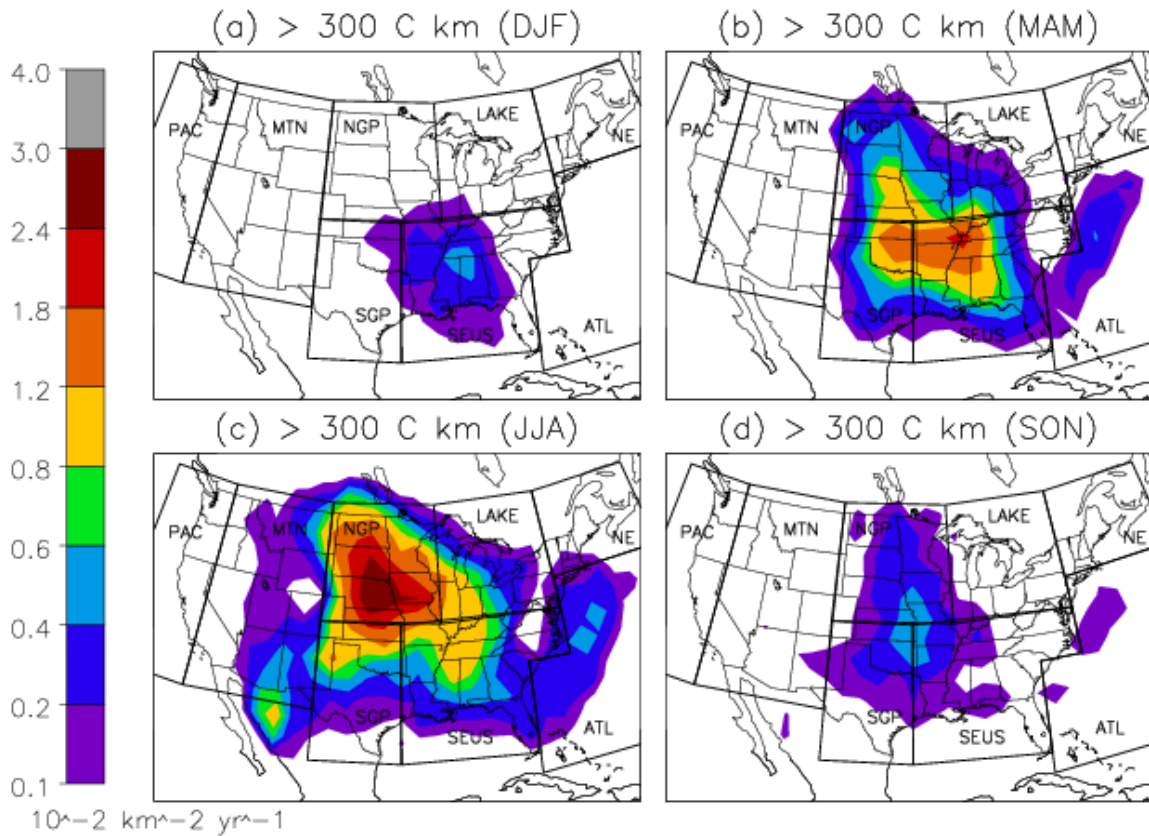


**Figure 5.** Annualized density maps for positive strokes with iCMC values greater than 300 C km, broken down by season for the period August 2007 through July 2012. (a) December through February (Winter). (b) March through May (Spring). (c) June through August (Summer). (d) September through November (Fall).

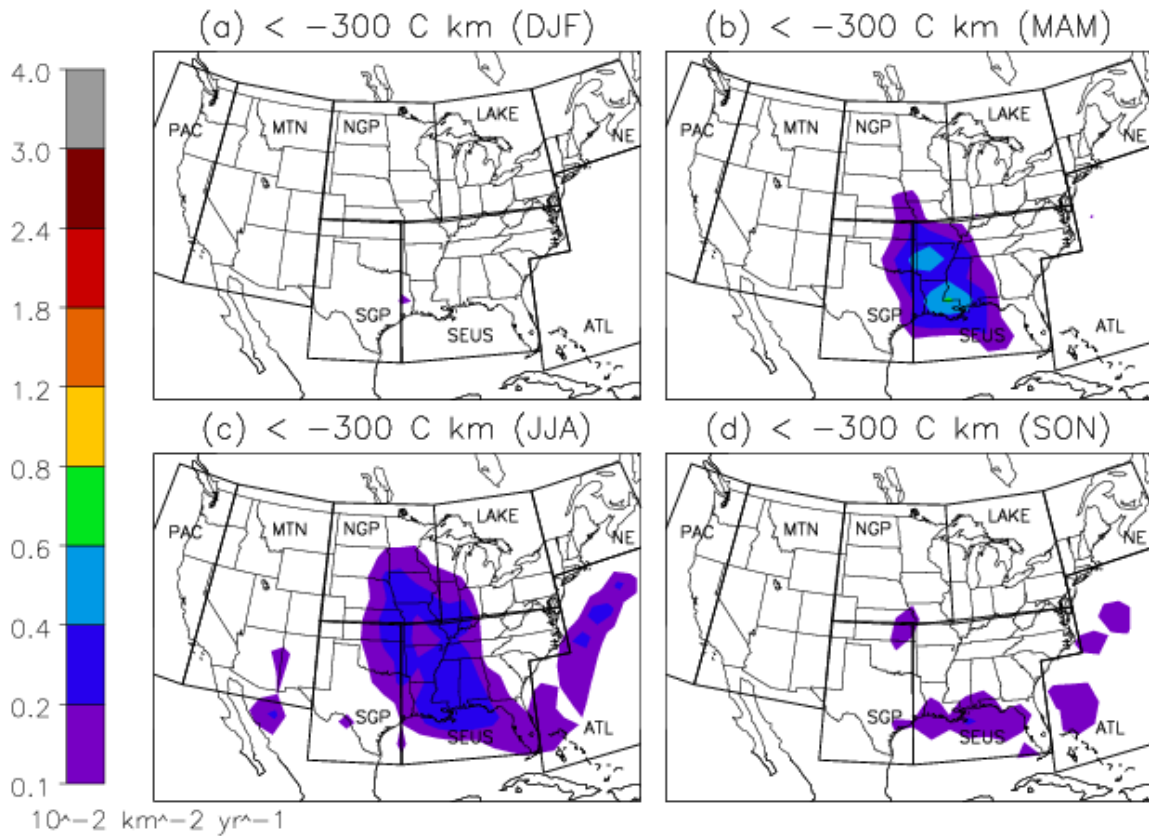


**Figure 6.** Annualized density maps for negative strokes with iCMC values greater than 300 C km, broken down by season for the period August 2007 through July 2012. (a) December through February (Winter). (b) March through May (Spring). (c) June through August (Summer). (d) September through November (Fall).

### *b. Regional diurnal distributions of large-iCMC CG lightning*

Fig. 7 shows diurnal distributions for all regions labeled in Fig. 1. Overall, a strong diurnal trend is present in all regions, with large negative iCMCs typically peaking prior to positive iCMCs. Sprite-class iCMCs ( $> 300$  C km) are predominantly positive (Fig. 8). In addition, the 100 C km peak for both polarities occurs earlier than the 300 C km peak. Results from each region for both thresholds ( $>100$  C km and  $>300$  C km) are summarized below.

Starting along the West Coast in the PAC region (Figs. 7a and 8a), large iCMCs are predominantly positive, with a diurnal peak around 2000 local solar time (LST) for both  $>100$  and  $>300$  C km plots. The NLDN peak (dashed lines; 1600 LST) is several hours before the iCMC peak. Despite the greater frequency of -CG lightning overall, +CGs dominate the large-iCMC population for both  $>100$  and  $>300$  C km distributions, seen in Table 1.

Moving eastward, the MTN region features a very strong diurnal signal in iCMC activity for both thresholds. The peak in  $>100$  C km (Fig. 7b) total iCMC activity occurs around 1500 LST, with negatives peaking around 1200 LST and positives peaking around 1700 LST, with a nearly complete cutoff in iCMC activity by 0000-0100 LST. Though temporally shifted, the positive and negative distributions are fairly even in terms of magnitude. The 300 C km distribution (Fig. 8b) is dominated by positives. It features a similar but much smaller peak in negative iCMCs before positives around 1400 LST, and a broad peak from 1600 LST onward to a sharp nocturnal peak around 2000 LST in positives. The peak in NLDN CGs is coincident with the peak of the total iCMC activity for 100 C km, around 1500 LST.

The NGP region, Figs. 7c and 8c, features predominantly positive large iCMCs, with a well-defined nocturnal peak from 1900-2000 LST again, despite the relative dominance of -CGs overall. The >300 C km curve again shifts later into the night, with a broad peak in iCMC activity from 2000 to 0200 LST. Total NLDN CG activity was generally coincident with total >100 C km activity temporally.

Moving eastward, the LAKE region distributions (Figs. 7d and 8d) feature a similar nocturnal peak and positive tendency as the NGP region, except the peak in 100 C km activity is much broader and stretches from approximately 1900 LST to 0300 LST. The 300 C km plot follows the same behavior. The NLDN CG peak is well before both large-iCMC peaks, occurring at approximately 1600 LST.

The SGP region (Figs. 7e and 8e) features a slightly less pronounced diurnal peak as the NGP and LAKE regions, with a peak in all CGs coinciding with the total >100 C km iCMC peak at approximately 1900 LST. Negatives rise slightly before positives in the >100 C km plot, and have a slight rise to a secondary peak around 0300 LST despite the decline in positive iCMC activity after the peak around 1900 LST. In the >300 C km plot, the nocturnal shift is again apparent, with an initial positive-dominated peak around 2000 LST, with a broad decrease until 0200 LST. Total NLDN CGs again peak around 1600 LST.

Large-iCMCs observed in the SEUS region tended to be negative compared to positive, with the total and negative iCMC peak in >100 C km (Fig. 7f) coming around 1400-1500 LST. Positive iCMCs peak much later, around 1900 LST. A more defined secondary negative peak, around 0300-0400 LST, also can be observed in the >100 C km plot. In the >300 C km plot (Fig. 8f), the large-iCMCs become characteristically more positive and nocturnal, with the peak in iCMC activity coming around 1900 LST,

and a broad decline until slight peak around 0300 LST. The NLDN peak is nearly coincident with the >100 C km distribution, with CGs peaking around 1500 LST.

The NE large-iCMC distributions (Figs. 7g and 8g) are positive-dominated with a temporally ill-defined peak in iCMC activity, but generally more large iCMCs occur in the local afternoon-evening than morning. The peak is broad in the >100 C km plot, as in the LAKE region, occurring during 2000-0400 LST. The broad >300 C km peak is also between these approximate hours. Total NLDN CGs peak around 1500-1600 LST in this region.

Oceanic ATL observations present a shift from the predominantly land-based domains. The >100 C km plot (Fig. 7h) is highly negative, with a broad morning peak from 0300 to 0700 LST. Large-iCMC positives again peak later than the negatives. The >300 C km peak (Fig. 8h) is more highly positive, and peaks later than the 100 C km plot, with a broad maximum during 0700-1300 LST. NLDN CGs peak at 0600 LST, nearly coinciding temporally with the >100 C km iCMC peak.

Overall, the NLDN CG observations show a strong diurnal signal, with most continental regions peaking in CG activity by 1600 LST. The NLDN activity peaks occur before the maxima in total iCMC activity in all regions. In general, there is a much greater possibility for a +CG to have a large or sprite-class iCMC compared to a -CG in all regions (Table 2). The NGP region has a relatively higher ratio of large iCMCs to all CGs, especially in positives. Also seen in Table 2, the percentages of sprite-class iCMCs to large iCMCs are much higher for positive strokes than negative strokes.

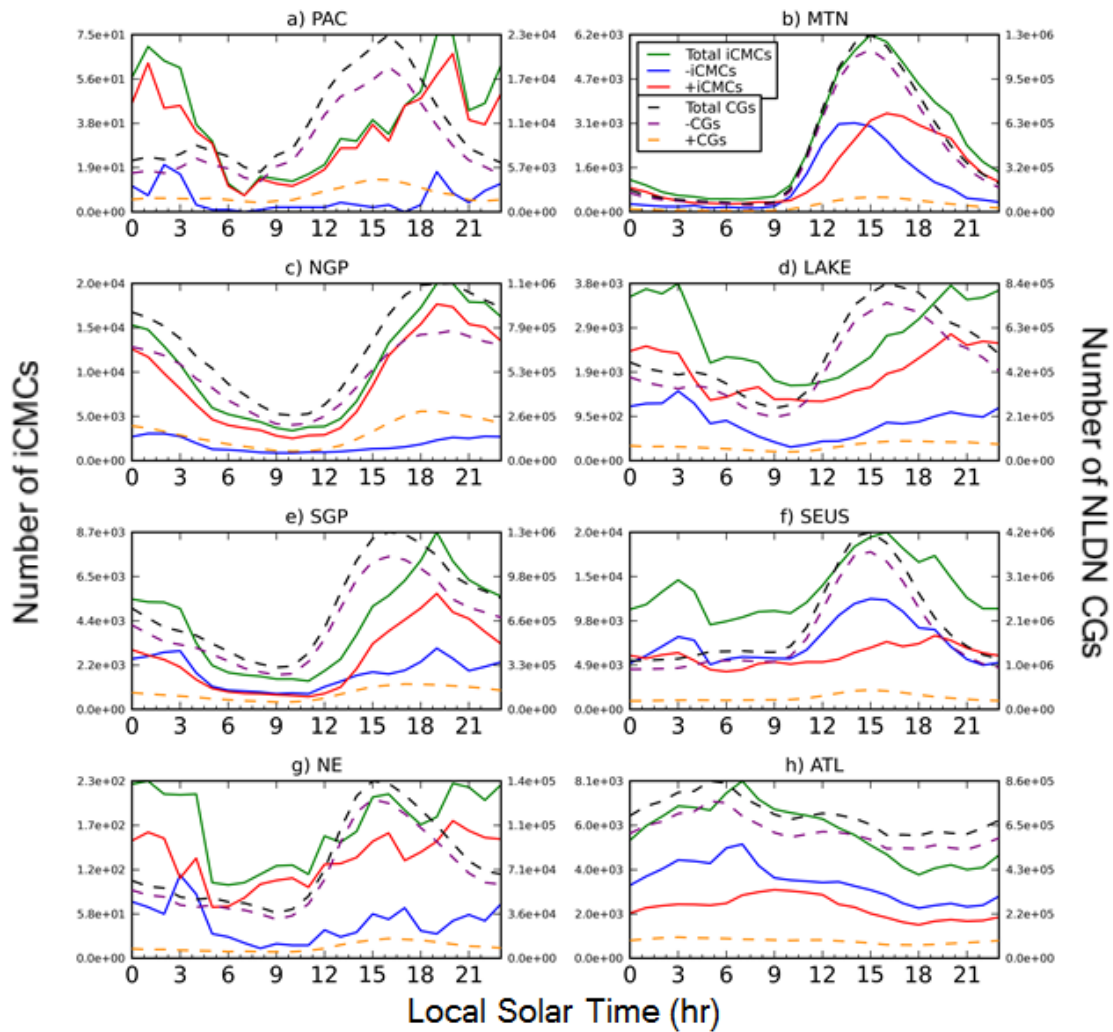


**Figure 7.** Diurnal distributions of regional iCMC events greater than 100 C km, for the period August 2007- December 2012. (a) Pacific Coast (PAC). (b) Intermountain West (MTN). (c) Northern Great Plains (NGP). (d) Great Lakes (LAKE). (e) Southern Great Plains (SGP). (f) Southeastern United States (SEUS). (g) New England (NE). (h) Atlantic Ocean (ATL).

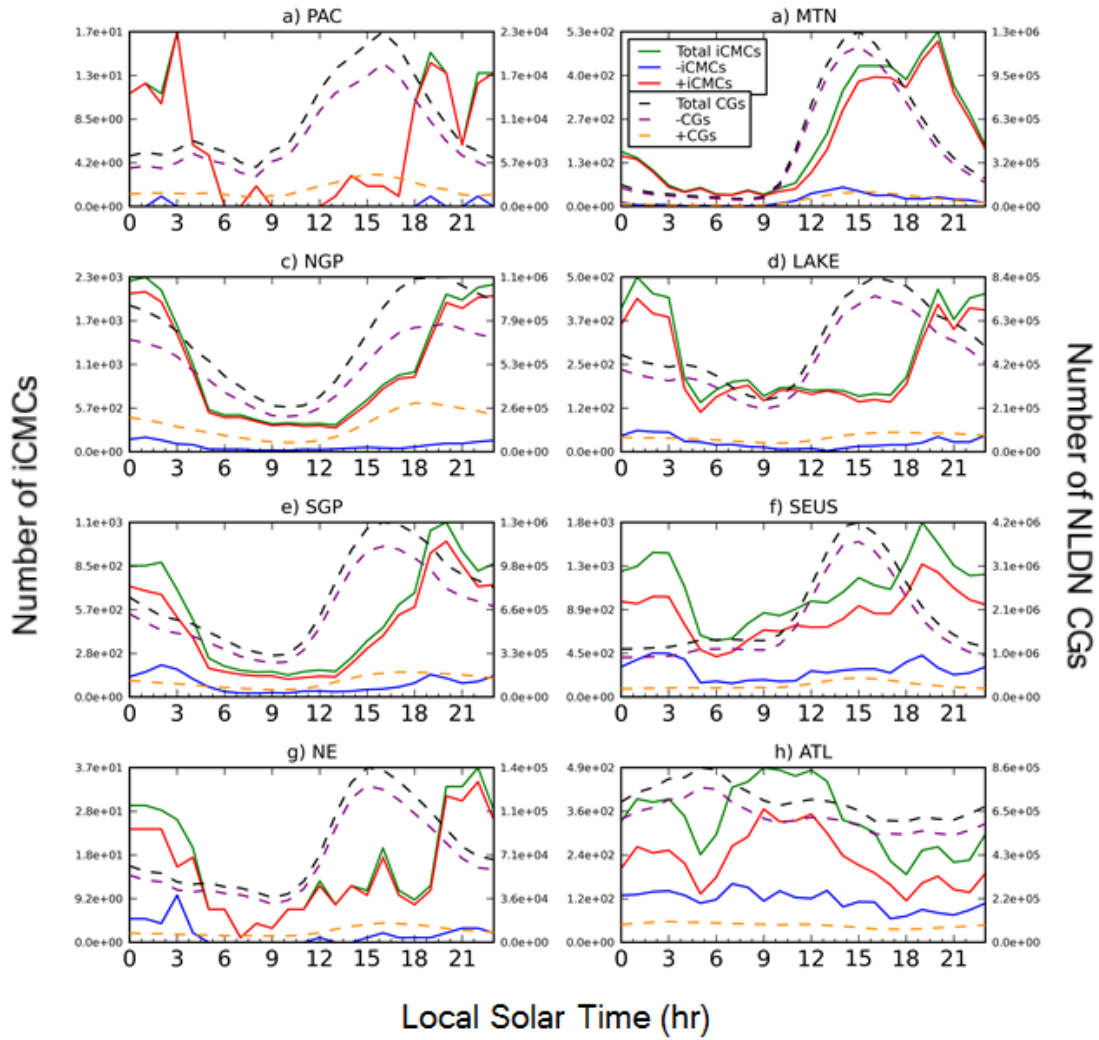


Figure 8. Same as in Fig. 8, but for iCMC events greater than 300 C km.

**Table 1.** Tabulation of total iCMC and NLDN CG statistics in each region for the time period August 2007-July 2012.

| Region | Large iCMCs > 100 C km |          |          | Sprite Class iCMCs >300 C km |          |          | NLDN CGs  |         |          |
|--------|------------------------|----------|----------|------------------------------|----------|----------|-----------|---------|----------|
|        | Total                  | Positive | Negative | Total                        | Positive | Negative | Total CGs | +CGs    | -CGs     |
| PAC    | 946                    | 813      | 133      | 143                          | 140      | 3        | 267896    | 53099   | 214797   |
| MTN    | 57907                  | 33625    | 24282    | 5132                         | 4669     | 463      | 10691221  | 1050164 | 9641057  |
| SGP    | 102130                 | 59462    | 42668    | 12623                        | 10598    | 2025     | 18266804  | 2873981 | 15392823 |
| NGP    | 257094                 | 213858   | 42236    | 27129                        | 25316    | 1813     | 16414208  | 3971396 | 12442812 |
| LAKE   | 65159                  | 45400    | 19759    | 6568                         | 5938     | 630      | 12506941  | 1672289 | 10834652 |
| SEUS   | 322935                 | 143254   | 179681   | 26962                        | 20376    | 6586     | 48746085  | 6717658 | 42028427 |
| NE     | 4206                   | 3100     | 1106     | 395                          | 352      | 43       | 1833198   | 216548  | 1616650  |
| ATL    | 137804                 | 54982    | 82822    | 8316                         | 5533     | 2783     | 16804163  | 2027868 | 14776295 |

**Table 2.** Ratios of large iCMC (>100 C km) activity to NLDN CG activity, sprite-class (>300 C km) iCMC activity to NLDN CG activity, and sprite-class iCMC activity to large iCMC activity in each region for the time period August 2007-July 2012.

| Region | Large iCMCs/ NLDN CGs |           |           | Sprite Class iCMCs/ NLDN CGs |           |           | Sprite Class iCMCs/ Large iCMCs |           |           |
|--------|-----------------------|-----------|-----------|------------------------------|-----------|-----------|---------------------------------|-----------|-----------|
|        | Total Ratio           | Positives | Negatives | Total Ratio                  | Positives | Negatives | Total Ratio                     | Positives | Negatives |
| PAC    | 0.35%                 | 1.53%     | 0.06%     | 0.05%                        | 0.26%     | 0.001%    | 15.12%                          | 17.22%    | 2.26%     |
| MTN    | 0.54%                 | 3.20%     | 0.25%     | 0.05%                        | 0.44%     | 0.005%    | 8.86%                           | 13.89%    | 1.91%     |
| SGP    | 0.56%                 | 2.07%     | 0.28%     | 0.07%                        | 0.37%     | 0.01%     | 12.36%                          | 17.82%    | 4.75%     |
| NGP    | 1.57%                 | 5.38%     | 0.34%     | 0.17%                        | 0.64%     | 0.01%     | 10.55%                          | 11.84%    | 4.29%     |
| LAKE   | 0.52%                 | 2.71%     | 0.18%     | 0.05%                        | 0.36%     | 0.01%     | 10.08%                          | 13.08%    | 3.19%     |
| SEUS   | 0.66%                 | 2.13%     | 0.43%     | 0.06%                        | 0.30%     | 0.02%     | 8.35%                           | 14.22%    | 3.67%     |
| NE     | 0.23%                 | 1.43%     | 0.07%     | 0.02%                        | 0.16%     | 0.003%    | 9.39%                           | 11.35%    | 3.89%     |
| ATL    | 0.82%                 | 2.71%     | 0.56%     | 0.05%                        | 0.27%     | 0.02%     | 6.03%                           | 10.06%    | 3.36%     |

## Discussion and Conclusions

Cummer et al. (2013) offered some general interpretations regarding the geographic distribution of large-iCMC positive lightning in terms of the behavior of mesoscale precipitation systems. This study's results support that general conclusion with additional evidence and justification, provided below.

The presence of a broad maximum in large positive iCMCs in the Central Plains (e.g., Nebraska) is notable, as this region is well known to be associated with broad maxima in mesoscale convective complexes (MCCs; Maddox 1980), including track locations, the fraction of annual and warm-season precipitation produced by (often nocturnal) MCCs, as well as cold cloud top frequency (Fritsch et al. 1986, McAnelly and Cotton 1989, Ashley et al. 2003). This region also is well known to contain broad maxima in +CG percentage, peak current, and multiplicity along with broad minima in the corresponding -CG characteristics (Lyons et al. 1998, Orville and Huffines 2001, Zajac and Rutledge 2001, Rudlosky and Fuelberg 2010, Orville et al. 2011). Additionally, this region contains a relative maximum in IC-to-CG lightning ratio (Boccippio et al. 2001). Many studies also have documented the northwestward march of MCC tracks (Velasco and Fritsch 1987, Augustine and Howard 1991, Ashley et al. 2003), CGs (Holle et al. 2011), and total lightning (Christian et al. 2003) from the southeastern United States into the Central Plains as seasons transition from winter to spring to summer. This behavior is also observed in the large-iCMC lightning data for both polarities.

It is therefore reasonable to infer that MCCs and MCSs, with their ability to produce high lightning flash rates (Goodman and MacGorman 1986, Carey et al. 2005,

Lang and Rutledge 2008, Makowski et al. 2013), and an enhanced percentage of +CG lightning in their stratiform regions (Orville et al. 1988, Rutledge and MacGorman 1988, Rutledge et al. 1990, MacGorman and Morgenstern 1998), play a significant role in the presence of many of these regional features. Given the known link between MCSs and the production of sprites (Boccippio et al. 1995, Lyons 1996, 2006, Lyons et al. 2003, Williams and Yair 2006, Lang et al. 2010), and the known link between sprite occurrence and large-CMC discharges (Wilson 1925, Boccippio et al. 1995, Huang et al. 1999, Hu et al. 2002, Cummer and Lyons 2005, Lyons et al. 2009, Lang et al. 2011a, Qin et al. 2012), the approximate collocation of the large-iCMC positive maximum with other lightning- and storm-related maxima in the Central Plains (NGP, SGP, LAKE) is thus expected.

The present study supports the conclusions of Cummer et al. (2013) that a slight eastward bias exists for stroke density of +CGs with  $> 300$  C km when compared to ones with  $> 100$  C km, particularly for the Central Plains. This is consistent with the composite-MCC life cycle study of McAnelly and Cotton (1989), which found that MCCs on average grow in size and reach full maturity eastward of central Nebraska. The nocturnal peak in large positive iCMCs is also most clearly associated with upscale development of MCSs (McAnelly and Cotton 1989). Larger (sprite-class) iCMCs are favored nocturnally as MCS stratiform regions develop and expand during this time period, allowing for a larger positive charge reservoir in the stratiform region (Boccippio et al. 1995, Williams 1998, Lyons 1996, 2006, Lyons et al. 2003, Williams and Yair 2006, Lang et al. 2010), and a greater frequency of larger iCMC positives would be expected (Cummer et al. 2013). Regionally, the LAKE region's more nocturnal peak in iCMC activity than NGP can be attributed to MCS advection from the NGP region

(McAnelly and Cotton 1989, Carbone et al. 2002). The distinct shift of the >300 C km iCMC maximum southeastward of the maximum in overall CG activity and >100 C km iCMC activity (Boccippio et al. 2001, Orville et al. 2011) is also well attributed to the advection and maturation of MCSs and their associated stratiform charge reservoirs.

Two other secondary maxima in both polarities of large-iCMC lightning are notable, and both further solidify the inferred association between large-iCMC lightning and mesoscale precipitation systems. One is the increase in stroke density during summer over the southwestern United States and northwestern Mexico (MTN). As stated previously, this region is strongly affected by the North American Monsoon (Adams and Comrie 1997), and mesoscale systems produce a large fraction of the seasonal rainfall (Lang et al. 2007), much like the Central Plains. Convective development by strong daytime forcing is evident especially in the MTN region. Based on the observations, large negative iCMCs may be generally associated with areas of convective development, consistent with Lang et al. (2013). However, as storms mature and produce large anvils, some possibly interacting with each other, stratiform charge reservoirs similar to those in MCSs develop, and extending the conclusions from Orville et al. (1988), Rutledge and MacGorman (1988), Rutledge et al. (1990), and MacGorman and Morgenstern (1998), the enhanced large-iCMC positive signal in MTN suggests that the increased +CG activity associated with increased stratiform area becomes evident, perhaps also in part due to the end-of-storm oscillation process (Williams 1998, Pawar and Kumra 2007).

Additionally, the Gulf Stream (ATL) is associated with rainfall and lightning enhancement year round (Christian et al. 2003, Virts et al. 2013), in part due to increased cyclogenesis and the anchoring of large precipitation systems over the warm

ocean current (Minobe et al. 2008) as well as winter monsoon cold air advection (Price and King 2002). Diurnally, the ATL region shows a typical oceanic distribution of convection, with a morning maximum in iCMCs > 100 C km as well as CGs roughly coinciding with maxima in oceanic convection and precipitation found in oceanic MCSs and deep convective cores by Romatschke et al. (2010) to be around 0500-0800 local time. Liu and Zipser (2008) as well as Romatschke et al. (2010) noted broad stratiform coverage over oceanic regions by midday, consistent with the maximum in sprite-class positive iCMCs over the ATL region near local midday. The dip in iCMC activity at the peak of CG activity can be explained in part by recent work by T. Chronis et al. (noted by Lang et al. 2013), in which low flash rates may allow the buildup of large amount of charge that can be subsequently neutralized by a single stroke, leading to a large peak current and iCMC/CMC. This also supports speculation concerning the occurrence of sprites over the Gulf Stream (Price and King 2002).

The NE and PAC regions show very little iCMC activity compared to the other regions (Table 1). The NE region shows a very weak diurnal cycle, with the NLDN CG peak coming in mid-afternoon, similar to the SEUS region, but shows enhanced iCMC activity overnight, possibly suggesting that some MCSs originating in the LAKE region advect into the region overnight in a similar manner as NGP-LAKE advection (McAnelly and Cotton 1989). The PAC region is heavily positive iCMC-dominated; the amount of large iCMCs was so low that they appeared to be mostly isolated in nature, possibly associated with stratiform regions within extratropical cyclones making landfall on the Pacific Coast, especially in winter (Lang et al. 2011b, Lyons et al. 2012). In the NE, SGP, SEUS, LAKE, and PAC regions, a noticeable peak in negative iCMC activity was observed as overall activity began to decline near local dawn. All of these regions are

predominantly land, but contain some portion of ocean or very large bodies of water (Fig. 1), so a small modulation by oceanic diurnal convective tendencies (Liu and Zipser 2008, Romatschke et al. 2010) may be the explanation of these upticks in negative (and in some cases positive) iCMC activity, most notably the SEUS region. In the case of the LAKE region, the Great Lakes may have convective enhancement overnight (similar to Lake Victoria in Africa; Nicholson and Yin 2002), perhaps aided by the convergence of land breezes over the lakes (Passarelli and Braham 1981), as opposed to daytime suppression of convection over the lakes in summertime (Lyons 1966).

What remains difficult to explain is the regional offset between large negative iCMCs (dominating in the southeastern United States) and large positive iCMCs (dominating in the Central Plains), which is especially present during the summer months (June-August). Interestingly, this offset is not as pronounced during other seasons, or in other regions. For example, maxima in large-iCMC lightning of either polarity exist near the Kansas/Missouri border region during the fall. Also, such an offset is not seen over the Gulf Stream or in the North American Monsoon region. Moreover, large positive iCMCs are common in the Southeast during the winter months, when the main tracks of MCSs remain south of the Central Plains (e.g., Velasco and Fritsch 1987). Additionally, the occurrence of large iCMCs in these cold-season MCSs and in frontal systems with very large stratiform cloud shields has not been explored extensively.

Assuming this holds true for the broader population of strokes in this study, then the results would be consistent with convection situated mostly eastward of stratiform precipitation in the Central Plains (i.e., a preference for eastward-moving leading-line, trailing stratiform MCSs during summer; Parker and Johnson 2000), while southeastern

precipitation systems may not feature pronounced stratiform regions during summer, perhaps due to the influence of the sea-breeze in organizing convection along the Gulf Coast. For example, Lang et al. (2013) presented an example of a prolific large-iCMC - CG producing storm that was oriented parallel to the coast with no well-developed stratiform precipitation.

Diurnal curves of CGs match the findings of the NLDN diurnal distributions (sorted by LST, allowing for an excellent comparison) by Holle (2013), with a good agreement temporally on the peak of total CG activity in each region. The peaks in CG activity (Figs. 7 and 8), especially the nocturnal predisposition in the Northern Great Plains and mid-afternoon peaks over the Rockies and Southeastern US, are also supported by Holle (2013). The total CG peak still occurs well before the iCMC peak temporally, with the majority of large-iCMC discharges coming while the CG peak is in its decline. The upscale development from convective cores into convective cores with adjoining stratiform is possibly an explanation, as flashes begin to tap larger charge reservoirs, and flash rates decrease such that the mechanism of charge neutralization by fewer, larger peak current and larger-iCMC flashes dominates (Chronis et al. 2013).

Clearly, these somewhat speculative hypotheses require further refinement and testing, in particular utilizing data from the national network of radars in the United States. The meteorology of systems producing large-iCMC lightning can further support the development of conclusions regarding large-iCMC production, most notably the link between stratiform charge reservoirs in MCSs as well as the association of large negative iCMCs with areas of convection. The size of the system may be important for whether it produces more or greater magnitude iCMC discharges than smaller systems,

and may affect preferred polarities. Analysis of individual iCMC-producing storms is currently underway.

### **Acknowledgements**

The authors gratefully acknowledge the support of Vaisala, Inc. in providing the National Lightning Detection Network Data on which the CMCN is built as well as the support of the Missile Defense Agency SBIR Program. NSF provided support for this work under Grant AGS-1010657, and DARPA provided additional funding support under the Nimbus program. The authors also would like to extend thanks to the Radar Meteorology Group at Colorado State University for valuable scientific input, and especially Paul Hein for invaluable computing support. The views, opinions, and findings in this report are those of the authors, and should not be construed as an official NASA or U.S. Government position, policy, or decision.

## Section 1 References

- Adams, D. K. and A. C. Comrie, 1997: The North American Monsoon. *Bull. Amer. Meteor. Soc.*, **78**, 2197-2213.
- Augustine, J. A. and K. W. Howard, 1991: Mesoscale Convective Complexes over the United States during 1986 and 1987. *Mon. Wea. Rev.*, **119**, 1575-1589.
- Ashley, W. S., T. L. Mote, P. G. Dixon, S. L. Trotter, E. J. Powell, J. D. Durkee, A. J. Grundstein, 2003: Distribution of Mesoscale Convective Complex Rainfall in the United States. *Mon. Wea. Rev.*, **131**, 3003-3017.
- Badan-Dangon, A., C.E. Dorman, M.A. Merrifield, and C.D. Winant, 1991: The Lower Atmosphere over the Gulf of California. *J. Geophys. Res.*, **96**(C9), 16877-16896.
- Boccippio, D.J., E.R. Williams, S.J. Heckman, W.A. Lyons, I.T. Baker, and R. Boldi, 1995: Sprites, ELF transients, and positive ground strokes. *Science*, **269**(5227), 1088-1091.
- Boccippio, D.J., K. L. Cummins, H. J. Christian, and S. J. Goodman, 2001: Combined Satellite- and Surface-Based Estimation of the Intracloud-Cloud-to-Ground Lightning Ratio over the Continental United States. *Mon. Wea. Rev.*, **129**, 108-122.
- Carbone, R.E., J.D. Tuttle, D.A. Ahijevych, and S.B. Trier, 2002: Inferences of Predictability Associated with Warm Season Precipitation. *J. Atmos. Sci.*, **59**(13), 2033-2056.
- Carey, L. D., M. J. Murphy, T. L. McCormick, and N. W. S. Demetriades, 2005: Lightning location relative to storm structure in a leading-line, trailing-stratiform mesoscale convective system. *J. Geophys. Res.*, **110**, D03105, doi:10.1029/2003JD004371.

- Christian, H. J. et al., 2003: Global frequency and distribution of lightning as observed from space by the Optical Transient Detector. *J. Geophys. Res.*, **108**(D1), 4005, doi:10.1029/2002JD002347.
- Chronis, T., R. Said, W. Koshak, E. Williams, E. Grant, E. McCaul, and K. Cummins, 2013: New Evidence on the Diurnal Variability of Peak Current in Global CG Lightning, *Bull. Amer. Meteor. Soc.*, submitted.
- Cummer, S. A. and U.S. Inan, 2000: Modeling ELF radio atmospheric propagation and extracting lightning currents from ELF observations. *Radio Science*, **35**(2), 385-394.
- Cummer, S. A. and M. Fullekrug, 2001: Unusually intense continuing current in lightning produces delayed mesospheric breakdown. *Geophys. Res. Lett.*, **28**(3), 495-498.
- Cummer, S.A. and W.A. Lyons, 2004: Lightning charge moment changes in US High Plains thunderstorms. *Geophys. Res. Lett.*, **31**(5), L05114.
- Cummer, S.A., and W.A. Lyons, 2005: Implications of lightning charge moment changes for sprite initiation. *J. Geophys. Res.*, **110**(A04304), doi:10.1029/2004JA010812.
- Cummer, S.A., W.A. Lyons, and M.A. Stanley, 2013: Three Years of Lightning Impulse Charge Moment Change Measurements in the United States. *J. Geophys. Res.*, **118**, 5176-5189, doi:10.1002/jgrd.50442.
- Cummins, K.L. and M.J. Murphy, 2009: An Overview of Lightning Locating Systems: History, Techniques, and Data Uses, with an In-Depth Look at the U.S. NLDN. *IEEE Trans. Elec. Comp.*, **51**(3), 499-518.
- Cummins, K.L., M.J. Murphy, E.A. Bardo, W.L. Hiscox, R.B. Pyle, and A.E. Pifer, 1998a: A Combined TOA/MDF Technology Upgrade of the U.S. National Lightning Detection Network. *J. Geophys. Res.*, **103**(D8), 9035-9044.

- Curran, E.B., R.L. Holle, and R.E. Lopez, 2000: Lightning Casualties and Damages in the United States from 1959 to 1994. *J. Climate*, **13**, 3448-3464.
- Franz, R.C., R.J. Nemzek, and J.R. Winckler, 1990: Television image of a large upward electrical discharge above a thunderstorm system. *Science*, **249**(4964), 48-51.
- Fritsch, J.M., R.J. Kane, and C.R. Chelius, 1986: The Contribution of Mesoscale Convective Weather Systems to the Warm-Season Precipitation in the United States. *J. Climate & App. Met.*, **25**(10), 1333-1345.
- Goodman, S. J., D. R. MacGorman, 1986: Cloud-to-Ground Lightning Activity in Mesoscale Convective Complexes. *Mon. Wea. Rev.*, **114**, 2320-2328.
- Hobbs, P.V., 1987: The Gulf Stream Rainband. *Geophys. Res. Lett.*, **14**(11), 1142-1145.
- Holle, R. L., K. L. Cummins, and N. W.S. Demetriades, 2011: Monthly distributions of NLDN and GLD360 cloud-to-ground lightning. *5<sup>th</sup> Conf. on the Meteorological Applications of Lightning Data*, American Meteorological Society, Seattle, WA. <https://ams.confex.com/ams/91Annual/webprogram/5LIGHTNING.html>.
- Holle, R.L., 2013: Diurnal Variations of NLDN Cloud-to-Ground Lightning in the United States. *6<sup>th</sup> Conf. on the Meteorological Applications of Lightning Data*, American Meteorological Society, Austin, TX.
- Hu, W., S.A. Cummer, W. A. Lyons, and T.E. Nelson, 2002: Lightning charge moment changes for the initiation of sprites. *Geophys. Res. Lett.*, **29**(8), 1279, doi:10.1029/2001GL014593.
- Huang, E., E. Williams, R. Boldi, S. Heckman, W. Lyons, M. Taylor, T. Nelson, and C. Wong, 1999: Criteria for sprites and elves based on Schumann resonance observations. *J. Geophys. Res.*, **104**(D14), 16943-16964.

- Lang, T. J., D. A. Ahijevych, S. W. Nesbitt, R. E. Carbone, S. A. Rutledge, R. Cifelli, 2007: Radar-observed characteristics of precipitating systems during NAME 2004. *J. Climate*, **20**, 1713-1733.
- Lang, T. J., and S. A. Rutledge, 2008: Kinematic, microphysical, and electrical aspects of an asymmetric bow-echo mesoscale convective system observed during STEPS 2000. *J. Geophys. Res.*, **113**, D08213, doi:10.1029/2006JD007709.
- Lang, T. J., W. A. Lyons, S. A. Rutledge, J. Meyer, D. R. MacGorman, and S. A. Cummer, 2010b: Transient luminous events above two mesoscale convective systems: Storm structure and evolution. *J. Geophys. Res.*, **115**, A00E22, doi:10.1029/2009JA014500.
- Lang, T. J., J. Li, W. A. Lyons, S. A. Cummer, S. A. Rutledge, and D. R. MacGorman, 2011a: Transient luminous events above two mesoscale convective systems: Charge moment change analysis. *J. Geophys. Res.*, **116**, A10306, doi:10.1029/2011JA016758.
- Lang, T. J., W. A. Lyons, S. A. Cummer, S. Rutledge, and T. E. Nelson, 2011b: Toward a climatology of precipitating systems that produce lightning with large impulse charge moment changes. *5<sup>th</sup> Conf. on the Meteorol. Appl. of Lightning Data*, Seattle, WA, Amer. Meteor. Soc., 4.3, <https://ams.confex.com/ams/91Annual/webprogram/Paper184639.html>.
- Lang, T. J., S. A. Cummer, S. A. Rutledge, and W. A. Lyons, 2013: The meteorology of negative cloud-to-ground lightning strokes with large charge moment changes: Implications for negative sprites. Accepted in *J. Geophys. Res. Atmos.*

- Liu, C. and E.J. Zipser, 2008: Diurnal cycles of precipitation, clouds, and lightning in the tropics from 9 years of TRMM observations. *Geophys. Res. Lett.*, **35**, L04819, doi:10.1029/2007GL0320437.
- Lyons, W.A., 1966: Some effects of Lake Michigan on squall lines and summertime convection, Proceedings of the 9<sup>th</sup> Conf. Great lakes Res., University of Michigan, Ann Arbor, MI, 259-273.
- Lyons, W. A., 1996: Sprite observations above the U.S. High Plains in relation to their parent thunderstorm systems. *J. Geophys. Res.*, **101**, 29,641-29,652.
- Lyons, W. A., M. Uliasz, and T.E. Nelson, 1998: Large Peak Current Cloud-to-Ground Lightning Flashes during the Summer Months in the Contiguous United States. *Mon. Wea. Rev.*, **126**, 2217-2233.
- Lyons, W. A., T. E. Nelson, E. R. Williams, S. A. Cummer, and M. A. Stanley, 2003: Characteristics of sprite-producing positive cloud-to-ground lightning during the 19 July 2000 STEPS mesoscale convective systems. *Mon. Wea. Rev.*, **131**, 2417-2427.
- Lyons, W. A., 2006: The meteorology of transient luminous events - An introduction and overview. *NATO Advanced Study Institute on Sprites, Elves and Intense Lightning Discharges*, M. Fullekrug et al. (eds.), Springer, 19-56.
- Lyons, W.A. and S.A. Cummer, 2008: Stratospheric Lightning: Forecasting and Nowcasting Tools. Final Report, SBIR Phase II, Missile Defense Agency, Contract HQ0006-06-C-7313, FMA Research, Inc., Fort Collins, CO, 298 pp.
- Lyons, W. A., M. Stanley, J. D. Meyer, T. E. Nelson, S. A. Rutledge, T. J. Lang, and S. A. Cummer, 2009: The meteorological and electrical structure of TLE-producing convective storms. In *Lightning: Principles, Instruments and Applications*, H.D.

- Betz et al. (eds.), 389-417 pp., Springer Science+Business Media B.V., DOI: 10.1007/978-1-4020-9079-0\_17.
- Lyons, W.A., T.A. Warner, S.A. Cummer, S.A. Rutledge, T.J. Lang, T.C. Meyer, G. Lu, T.E. Nelson, and T. Samaras, 2012: Different Strokes: Researching the Unusual Lightning Discharges Associated with Sprites and Jets and Atypical Meteorological Regimes. Proceedings of the 22<sup>nd</sup> International Lightning Detection Conference, Boulder, Colorado, 1-4 April 2012, 19 pp.
- MacGorman, D. R., and C. D. Morgenstern, 1998:, Some characteristics of cloud-to-ground lightning in mesoscale convective systems. *J. Geophys. Res.*, **103**(D12), 14011-14023, doi:10.1029/97JD03221.
- Maddox, R. A., 1980: Mesoscale Convective Complexes. *Bull. Amer. Meteor. Soc.*, **61**, 1374-1387.
- Makowski, J. A., D. R. MacGorman, M. I. Biggerstaff, and W. H. Beasley, 2013: Total Lightning Characteristics Relative to Radar and Satellite Observations of Oklahoma Mesoscale Convective Systems. *Mon. Wea. Rev.*, **141**, 1593-1611.
- McAnelly, R. L. and W. R. Cotton, 1989: The Precipitation Life Cycle of Mesoscale Convective Complexes over the Central United States. *Mon. Wea. Rev.*, **117**, 784-808.
- Minobe, S., A. Kuwano-Yoshida, N. Komori, S.P. Xie, & R.J. Small, 2008: Influence of the Gulf Stream on the Troposphere. *Nature*, **452**(7184), 206-209.
- Nicholson, S.E. and X. Yin, 2002: Mesoscale patterns of rainfall, cloudiness, and evaporation over the Great Lakes of East Africa. *The East African Great Lakes: Limnology, Palaeolimnology, and Biodiversity*, **12**, 93-119.

- Orville, R. E., R.W. Henderson, and L.F. Bosart, 1988: Bipole patterns revealed by lightning locations in mesoscale storm systems. *Geophys. Res. Lett.*, **15**(2), 129-132.
- Orville, R.E., 1990: Winter Lightning Along the East Coast. *Geophys. Res. Lett.*, **17**(6), 713-715.
- Orville, R. E. and G. R. Huffines, 2001: Cloud-to-Ground Lightning in the United States: NLDN Results in the First Decade, 1989-98. *Mon. Wea. Rev.*, **129**, 1179-1193.
- Orville, R.E., G.R. Huffines, W.R. Burrows, and K.L. Cummins, 2011: The North American Lightning Detection Network (NALDN)- Analysis of Flash Data: 2001-09. *Mon. Wea. Rev.*, **139**(5), 1305-1321.
- Parker, M. D. and R. H. Johnson, 2000: Organizational Modes of Midlatitude Mesoscale Convective Systems. *Mon. Wea. Rev.*, **128**, 3413-3436.
- Pasko, V.P., U.S. Inan, and T.F. Bell, 2001: Mesosphere-troposphere coupling due to sprites, *Geophys. Res. Lett.*, **28**(19), 3821-3824.
- Passarelli Jr., R.E., and R.R. Braham Jr., 1981: The role of the winter land breeze in the formation of Great Lake snow storms. *Bull. Amer. Meteor. Soc.*, **62**(4), 482-492.
- Pawar, S.D. and A.K. Kamra, 2007: End-of-storm oscillation in tropical air mass thunderstorms. *J. Geophys. Res.*, **112**, D03204, doi:10.1029/2005/JD006997.
- Price, C., W. Burrows, P. King, 2002: The likelihood of winter sprites over the Gulf Stream. *Geophys. Res. Lett.*, **29**, doi:10.1029/2002GL015571.
- Qin, J., S. J. Celestin, and V. P. Pasko, 2012: Minimum charge moment change in positive and negative cloud to ground lightning discharges producing sprites. *Geophys. Res. Lett.*, **39**, L22801, doi:10.1029/2012GL053951.

- Rakov, V.A. and M. A. Uman, 2003: *Lightning*. Cambridge University Press, Cambridge, 687 pp.
- Romatschke, U., S. Medina, and R.A. Houze, 2010: Regional, Seasonal, and Diurnal Variations of Extreme Convection in the South Asian Region. *J. Climate*, **23**, 419-439.
- Rudlosky, S. D. and H. E. Fuelberg, 2010: Pre- and Postupgrade Distributions of NLDN Reported Cloud-to-Ground Lightning Characteristics in the Contiguous United States. *Mon. Wea. Rev.*, **138**, 3623-3633.
- Rutledge, S. A., C. Lu, and D. R. MacGorman, 1990: Positive Cloud-to-Ground Lightning in Mesoscale Convective Systems. *J. Atmos. Sci.*, **47**, 2085-2100.
- Rutledge, S. A., D. R. MacGorman, 1988: Cloud-to-Ground Lightning Activity in the 10-11 June 1985 Mesoscale Convective System Observed during the Oklahoma-Kansas PRE-STORM Project. *Mon. Wea. Rev.*, **116**, 1393-1408.
- Sao Sabbas, F. T. et al., 2010: Observations of prolific transient luminous event production above a mesoscale convective system in Argentina during the Sprite2006 Campaign in Brazil. *J. Geophys. Res.*, **115**, A00E58, doi:10.1029/2009JA014857.
- Velasco, I., and J. M. Fritsch, 1987: Mesoscale convective complexes in the Americas. *J. Geophys. Res.*, **92**(D8), 9591-9613, doi:10.1029/JD092iD08p09591.
- Virts, K. S., J. M. Wallace, M. L. Hutchins, and R. H. Holzworth, 2013: Highlights of a new ground-based, hourly global lightning climatology. *Bull. Amer. Meteorol. Soc.*, In Press, doi: <http://dx.doi.org/10.1175/BAMS-D-12-00082.1>.
- Warner, T.A., 2011: Observations of simultaneous upward lightning leaders from multiple tall structures. *Atmos. Res.*, 2011, doi: 10.1016/j.atmosres.2011.07.004.

- Warner, T. A., K. L. Cummins, and R. E. Orville, 2012a: Upward lightning observations from towers in Rapid City, South Dakota and comparison with National Lightning Detection Network data, 2004-2010. *J. Geophys. Res.: Atmos.*, **117**, D19109, doi:10.1029/2012JD018346.
- Warner, T.A., M.M.F. Saba, S. Ridge, M. Bunkers, W. Lyons and R.E. Orville, 2012b: Lightning-triggered upward lightning from towers in Rapid City, South Dakota. Proceedings, ILDC, Boulder, CO, 9 pp.
- Williams, E.R., 1988: The positive charge reservoir for sprite-producing lightning, *J. Atmos. Solar-Terres. Phys.*, **60**, 689-692.
- Williams, E. R., V. Mushtak, D. Rosenfeld, S. Goodman, and D. Boccippio, 2005: Thermodynamic conditions favorable to superlative thunderstorm updraft, mixed phase microphysics and lightning flash rate. *Atmos. Res.*, **76**, 288- 306.
- Williams, E.R. and Y. Yair, 2006: The microphysical and electrical properties of sprite-producing thunderstorms. NATO Advanced Study Institute on Sprites, Elves and Intense Lightning Discharges, M. Fullekrug et al. (eds.), Springer, 57-83.
- Williams, E., et al., 2012: Resolution of the sprite polarity paradox: The role of halos. *Radio Sci.*, **47**, RS2002, doi:10.1029/2011RS004794.
- Wilson, C.T.R., 1925: The electric field of a thunderstorm and some of its effects. *Proc. Phys. Soc. Lond*, **37**, 32D-37D.
- Zajac, B. A. and S. A. Rutledge, 2001: Cloud-to-Ground Lightning Activity in the Contiguous United States from 1995 to 1999. *Mon. Wea. Rev.*, **129**, 999-1019.

## SECTION 2

### Radar Case Studies Synopsis

Results of eight case studies of Northern Great Plains mesoscale convective systems (MCSs) using the NMQ National Radar Mosaic dataset are presented. Thresholds of large (100-300 C km) and sprite-class (>300 C km) were used to disseminate impulse charge moment change (iCMC) discharges within the MCSs. A radar analysis algorithm on a 5-minute radar volume basis was developed, and included convective-stratiform partitioning, association of iCMCs and CGs to their respective storms, and statistical analysis on large (100-300 C km) and sprite-class (>300 C km) iCMC-producing storms.

Results from these case studies indicated a strong preference of sprite-class iCMCs to be positive and located in stratiform-identified regions. A 2-3 hour delay in the maximum activity of sprite-class iCMCs after the maximum large iCMC activity was noted, and was strongly correlated with the maximum areal coverage of stratiform area as well as the propagation of the MCS eastward. A loose correlation between more frequent sprite-class iCMC production and larger stratiform areas was noted, suggesting that larger stratiform areas are simply more capable, not more likely, to produce high sprite-class iCMC rates.

Enhanced maximum convective echo heights corresponded to enhanced sprite-class iCMC activity in stratiform areas, attributed in part to enhanced charge advection from the convective line. In situ charging was also presumed to have a significant role in charge generation leading to sprite-class iCMC discharges in stratiform regions.

## Introduction

Supporting the findings in Section 1 are case studies based on radar observations of mesoscale convective systems (MCSs). MCSs provide a large amount of rainfall to many locations in midlatitudes (Maddox 1980, Fritsch et al. 1986, McAnelly and Cotton 1989) as well as the tropics (Miller and Fritsch 1991, Mapes 1993). They come in many shapes and sizes structurally (Parker and Johnson 2000), but fundamentally have an area with of convection with adjoining stratiform precipitation (Houze 1989). Their lifetimes range from several hours to nearly a day and often advect across hundreds of kilometers (McAnelly and Cotton 1989). Under these criteria, most warm-season MCSs fall under the classification of leading-line trailing stratiform (LLTS), with mean front-to-rear mesoscale flow at upper levels (Parker and Johnson 2000). Electrically, MCSs are typically characterized by frequent lightning (Goodman and MacGorman 1986, Carey et al. 2005, Lang and Rutledge 2008, Makowski et al. 2013) and an expansive positive charge layer near the melting level (Stolzenburg et al. 1994, 1998a, Shepherd et al. 1996, Williams 1998, Schuur and Rutledge 2000b, Lyons et al. 2003) and a radar brightband (Rutledge et al. 1988, Zhang et al. 2008) indicating the melting of ice. However, the location of various charge layers in the stratiform shield can vary from storm to storm (Marshall and Rust 1993, Lang et al 2010b). It is also well-known that the majority of cloud-to-ground strokes (CGs) within the stratiform region are positive, generated by the positive charge layer near the freezing level (Rutledge and MacGorman 1988, Rutledge et al. 1990, Williams 1998, Carey et al. 2003, 2005, Lang et al. 2004, Lang and Rutledge 2008, Lang et al. 2010b, 2011a), commonly with very

large peak currents (Lyons et al. 1998). Thus, the magnitude of charge within various positive charge reservoirs is of particular interest for stratiform lightning.

Since the serendipitous discovery of mesospheric sprites with low-light cameras pointed above Minnesota thunderstorms (Franz et al. 1990), their association with MCSs, in particular with very energetic positive CGs in the stratiform region has been well documented (Boccippio et al. 1995, Lyons 1996, Williams 1998, Lyons et al. 2003, 2009, Lang et al. 2010b, 2011a, Section 1). A metric for relating sprite production to a CG stroke, charge moment change (CMC; Cummer and Inan 2000), has been utilized by many studies (Boccippio et al. 1995, Huang et al. 1999, Pasko et al. 2001, Hu et al. 2002, Cummer and Lyons 2005, etc.), with the conclusion that a large magnitude CMC for a CG is very likely to produce a sprite. Impulse charge moment change (iCMC), the charge moment change over the first 2 ms, is more useful in real-time for diagnosing sprite probability (Lyons and Cummer 2008) (discussed in more detail in Section 1). The physical implications of large iCMCs (100-300 C km), which contain the lowest observed iCMC associated with a sprite (120 C km, Hu et al. 2002), and sprite-class iCMCs (> 300 C km), above which the probability of a sprite increases beyond 75-80% at 300 C km (Lyons et al. 2009), are discussed in more detail in Section 1. It should be noted that the type of lightning producing large and sprite-class iCMCs is exceptionally energetic and can loudly “ring” the earth-ionosphere cavity (Williams et al. 2012). Garden variety strokes can be shown to have an iCMC of around 10 C km (Section 1; after Rakov and Uman 2003).

Climatologies of large and sprite-class iCMCs have been conducted (Cummer et al. 2013, Section 1), providing a large-scale overview of the storm types that produce large and sprite-class iCMCs, thus allowing this study to hone in on MCSs and their

characteristics conducive to production of large and sprite-class iCMCs. To date, the only studies that have analyzed an MCS producing sprites are analyses of Oklahoma MCSs conducted by Lang et al. (2010b, 2011a), from which this study follows. More recently, Lang et al. (2013) delved into negative sprite production in the southeastern United States. However, a larger population of MCSs has not been sampled to produce more general conclusions regarding transient luminous event (TLE) production above the stratiform regions (sprites in particular). Previous studies (Schuur and Rutledge 2000b, Lang et al. 2004, Lang and Rutledge 2008, Lang et al. 2010b, 2011a) have discussed the relative contributions of two different charge generation mechanisms in the stratiform region of MCSs. Charge advection from the convective line (Rutledge and MacGorman 1988, Rutledge et al. 1990), and *in situ* non-inductive charging (Rutledge and Petersen 1994, Schuur and Rutledge 2000b) are believed to both have significant contributions to stratiform positive charge reservoirs. This study attempts to differentiate the relative contributions of these mechanisms towards the production of large and sprite-class iCMCs in a more generalized picture of warm-season MCSs, building on the conclusions drawn by Lang et al. (2010b, 2011a). This study extends the analysis in Lang et al. (2010b) to a larger population of MCSs, and provides some physical justification for the occurrence of large and sprite-class iCMCs within stratiform regions of MCSs.

## Data

In this chapter we describe three main data components used in this study: real-time data from the Charge Moment Change Network (CMCN), flash-level data from the National Lightning Detection Network (NLDN), and radar data from the National Mosaic Quantitative Precipitation Estimation (NMQ) dataset. Section 1 describes the iCMC and NLDN data in more detail, while the NMQ data are described here in more detail.

The NMQ radar mosaics draw on input dating back to 2009 from the nationwide network of S-Band NEXRAD radars within the United States (Zhang et al 2011). Fig. 9 shows the coverage of the NMQ radar data, as well as the individual tiles in the NMQ domain. For this study, MCSs on spatial scales typically larger than the domain of a handful of radars were analyzed. So the NMQ composite data were ideal for this application. The NMQ data field used was the MREF3D three-dimensional reflectivity mosaic, which is at  $0.01^\circ$  latitude/longitude ( $\sim 1$  km at middle latitudes) resolution, with 5-minute complete volumes (Zhang et al 2011). The radar vertical resolution is at 0.25 km, beginning at 0.5 km MSL, gradually stretching out to 0.5 km above 3 km MSL, and 1 km or more above 9 km MSL (Zhang et al. 2011).

## Methodology

In this chapter, we describe the general methodology utilized for analysis of radar data. Several MCS cases were selected for analysis based on iCMC maps produced and archived by W. Lyons and T. Nelson (personal communication with W. Lyons), as well as radar loops to confirm the presence of the MCS. The domain in which the MCSs were selected encompassed the NMQ mosaic tiles labeled 2-3-6-7 (Fig. 9), focusing primarily within the NGP region (Section 1). The MCSs were selected to be primarily of the leading-line, trailing stratiform morphology (Parker and Johnson 2000). As electrical behavior within warm-season MCSs can vary (Lang et al. 2010b), multiple months were chosen to get a more general picture of MCSs within the warm season. Since MCSs are primarily nocturnal in the Northern Great Plains (McAnelly and Cotton 1989; Section 1) and bisect the UTC date, two days of radar and NLDN data archived by UTC time were required to be ingested by the algorithm. Each timestep in the algorithm is 5 minutes, for a total of 288 per day, to correspond with the temporal resolution of the NMQ radar volumes (Zhang et al. 2011). Within each timestep of the algorithm, the real-time iCMC dataset, described in detail by Lyons and Cummer (2008) and Cummer et al. (2013), is queried to determine if a large iCMC ( $100 \text{ C km} > \text{iCMC} > 300 \text{ C km}$ ; see Section 1 for iCMC criteria descriptions) or sprite-class iCMC ( $> 300 \text{ C km}$ ) occurred within that radar volume. When the condition of a large-iCMC discharge occurring within the 5-minute volume and spatial domain is met, then the NLDN daily file is perused to locate all flashes within that 5-minute volume and 2-3-6-7 spatial domain.

For each 5-minute volume, the four three-dimensional radar reflectivity tiles were then stitched together, similar to Lang et al. (2013), to form a coherent, single grid for

analysis. The 3D reflectivity fields are much too large to undergo such a bulk analysis in a reasonable timeframe, so a constant-height reflectivity field at a height of 4 km was selected to perform analysis. The height of 4 km was selected to coincide with the typical location of the positive charge reservoir within deep precipitating stratiform regions in MCSs near the freezing level (Shepherd et al. 1996, Williams 1998, Lyons et al. 2003) and radar brightband (Rutledge et al. 1988, Zhang et al. 2008), which denotes the spatial extent of the heaviest stratiform precipitation within a MCS. IDL's `label_region` function was then employed on the 4 km reflectivity field to locate individual features (Lang et al. 2007, 2013) with a minimum reflectivity threshold of 10 dBZ. Features intersecting the borders of the NMQ Tile 2-3-6-7 domain (Fig. 9) were removed in order to produce analysis on a complete reflectivity feature for variables such as areas and feature echo tops.

After removal of border features, the 4 km reflectivity field then underwent convective-stratiform partitioning, similar to Guy et al. (2013), using values of  $a=12$  and  $b = 64$ , with convective core value minimum values of 47 dBZ, tuned for North American continental convection in the Yuter and Houze (1998) cosine averaging methodology. The NLDN flashes and iCMCs were then associated to their respective features with the feature and convective/stratiform masks. Once the iCMC-containing features were identified, basic spatial dimensions and rates (shown in Table 3) were calculated from those unique features, on a per 5-minute volume basis. One caveat to this method is that the radar volumes are at 5-minute resolution, while the iCMC and NLDN data are at second-of-day resolution, so some iCMCs and CGs could be incorrectly labeled as convective or stratiform, or be labeled in clear air, because of storm motion within the volume itself. After the raw data were output, a 1 hour moving average of feature

variables was employed to smooth out values that fluctuated due to situations such as an iCMC not occurring in 5 minute volume or multiple features containing large iCMCs.

**Table 3.** List of variables calculated from analysis of NMQ data.

| <b>Variable</b>                 | <b>Units</b>                |
|---------------------------------|-----------------------------|
| Total 10 dBZ Feature Area       | sq km                       |
| Convective-identified Area      | sq km                       |
| Stratiform Area > 10 dBZ        | sq km                       |
| 10 dBZ echo height              | km MSL                      |
| 20 dBZ echo height              | km MSL                      |
| 30 dBZ echo height              | km MSL                      |
| 40 dBZ echo height              | km MSL                      |
| 50 dBZ echo height              | km MSL                      |
| 60 dBZ echo height              | km MSL                      |
| Convective +CGs                 | # (5 min vol) <sup>-1</sup> |
| Convective -CGs                 | # (5 min vol) <sup>-1</sup> |
| Stratiform +CGs                 | # (5 min vol) <sup>-1</sup> |
| Stratiform -CGs                 | # (5 min vol) <sup>-1</sup> |
| Convective +iCMCs, large        | # (5 min vol) <sup>-1</sup> |
| Convective -iCMCs, large        | # (5 min vol) <sup>-1</sup> |
| Stratiform +iCMCs, large        | # (5 min vol) <sup>-1</sup> |
| Stratiform -iCMCs, large        | # (5 min vol) <sup>-1</sup> |
| Convective +iCMCs, sprite-class | # (5 min vol) <sup>-1</sup> |
| Convective -iCMCs, sprite-class | # (5 min vol) <sup>-1</sup> |
| Stratiform +iCMCs, sprite-class | # (5 min vol) <sup>-1</sup> |
| Stratiform -iCMCs, sprite-class | # (5 min vol) <sup>-1</sup> |

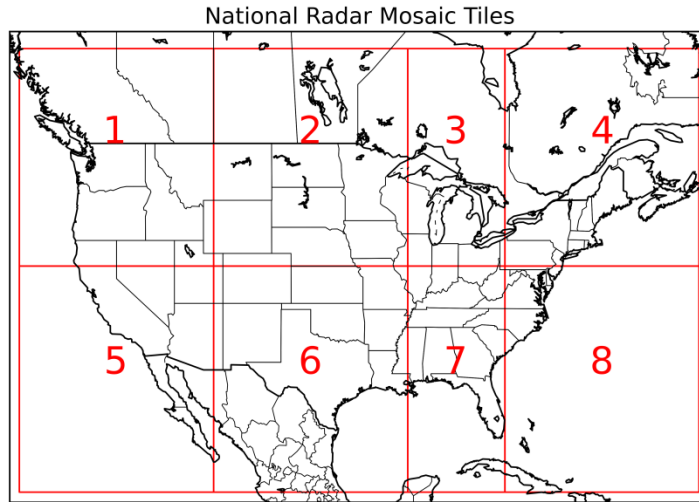


**Figure 9.** Areal coverage of the NMQ reflectivity mosaic tiles over the contiguous United States.

## Results

### *a. Overall Statistics*

A total of eight MCSs were analyzed, with an overview of the MCSs studied provided in Tables 4 and 5. Six of the eight MCSs were approximately the same size, with stratiform 10 dBZ echo areas near 150,000 km<sup>2</sup> at maximum extent (Table 4), and produced anywhere from 600-1200 large iCMCs over the course of their lifetimes. A smaller MCS, the 20110818 case, had a maximum stratiform area of 115,000 km<sup>2</sup>, while a very large MCS, the 20120614 case, had a stratiform area near 280,000 km<sup>2</sup>. The 20120614 case produced far and away the most large iCMCs and sprite-class iCMCs, as well as total CGs. A definitive relation between stratiform area and sprite-class iCMC production was not evident.

Looking at Table 4, the maximum height of convective echoes (40, 50, and 60 dBZ) approximately scaled with the total amount of CGs and large iCMCs in the MCS. The 20120615 and 20120705 cases illustrated this best, with the maximum height of the convective echoes being notably lower than the other MCS cases, corresponding to a notably lower total iCMC output. The amount of total CGs produced by the MCSs in both convective and stratiform regions did not scale linearly with the maximum height of the convective echoes, but the maximum 5-minute CG rate was loosely related to the maximum convective echo height.

The overall lightning statistics for the MCSs is shown in Table 5. Overall, the MCSs produced much more positive CGs and large positive iCMCs than negatives, consistent with the climatological findings of Cummer et al. (2013) and Section 1. Most CGs were confined to convective-identified areas (Fig. 10), and large iCMCs tended to also occur within or near convective regions more often than stratiform regions.

However, there was a strong tendency for sprite-class iCMCs to be located in stratiform regions, with nearly all sprite-class iCMCs being positive, again consistent with Cummer et al. (2013) and Section 1. A higher percentage of +CGs were located in stratiform regions than their negative counterparts, but overall, there were more CGs located in convective-identified regions than stratiform, by a ratio of no less than 2 :1, consistent with Rutledge and MacGorman (1988) and Rutledge et al (1990).

Interestingly, dividing the total number of sprite-class +iCMCs occurring in the stratiform by the total number of stratiform +CGs yielded a nearly constant ratio of approximately 3% (Table 6). Large +iCMC/+CG ratios yielded more variable statistics, such as approximately 6-20% of stratiform +CGs produced a large stratiform +iCMC across the eight MCSs. Negative iCMC/-CG ratios were much lower on average than positive iCMC/+CG ratios, consistent with Section 1 findings. Additionally, stratiform ratios for both large and sprite-class iCMCs to CGs were higher than convective ratios for both polarities.

A characteristic radar volume of an MCS (20120614) at peak maturity at  $z = 4$  km is shown in Fig. 10, just after 11 PM local time, as the MCS stretches from the southwestern reaches of Iowa through to northwestern Texas. Several sprite-class iCMCs are located deep within the stratiform region, upwards of  $2^\circ$  latitude (approx. 200 km) from the convective line. The convective line (outlined in white) is well-defined, though there are some spurious areas identified as convective deep within stratiform region; this is a function of the data's resolution, especially near WSR-88D radar sites (extending Steiner and Smith 2002). The brightband is also well-defined in a vertical cross-section through the stratiform region where three of the sprite-class iCMCs occurred (Fig. 11), trailing the convective line by approximately 20-30 km. The top of

the stratiform echo (10 dBZ) is approximately 12 km, and near 16 km for the convective core.

**Table 4.** Overview of MCS cases in terms of key variables shown in Table 1.

| Date     | MCS Location | Total large iCMCs (>100 C km) |            |            | Sprite Class iCMCs (>300 C km) |            |            | Total CGs | Max 5 min CG Rate | Max Areas (sq km) |            | Max Heights (km) |        |        |
|----------|--------------|-------------------------------|------------|------------|--------------------------------|------------|------------|-----------|-------------------|-------------------|------------|------------------|--------|--------|
|          |              | Total                         | Stratiform | Convective | Total                          | Stratiform | Convective |           |                   | Stratiform        | Convective | 40 dBZ           | 50 dBZ | 60 dBZ |
| 20110616 | CO/NE/SD     | 1101                          | 439        | 662        | 90                             | 70         | 20         | 14208     | 229               | 161872            | 17036      | 16.83            | 14.41  | 11.5   |
| 20110624 | NE/SD        | 1068                          | 444        | 624        | 120                            | 83         | 37         | 20143     | 336               | 150792            | 12326      | 16.64            | 14.44  | 11.08  |
| 20110704 | NE/SD        | 965                           | 203        | 762        | 135                            | 81         | 54         | 14616     | 245               | 147053            | 18188      | 17.82            | 15.28  | 10.86  |
| 20110818 | NE/IA/MO     | 922                           | 328        | 594        | 172                            | 109        | 63         | 22318     | 390               | 115508            | 14701      | 17.75            | 16.54  | 13.06  |
| 20120430 | KS/OK/MO     | 927                           | 349        | 579        | 133                            | 68         | 65         | 25745     | 417               | 152656            | 20391      | 18               | 15.58  | 11.25  |
| 20120614 | NE/KS/OK     | 1652                          | 866        | 786        | 279                            | 204        | 75         | 41256     | 613               | 278704            | 60465      | 18               | 16.19  | 12.19  |
| 20120615 | NE/SD        | 647                           | 352        | 295        | 56                             | 42         | 14         | 7308      | 176               | 158316            | 14281      | 15               | 11.71  | 8.99   |
| 20120705 | SD/ND        | 683                           | 321        | 362        | 77                             | 53         | 24         | 14159     | 327               | 155291            | 18450      | 16.63            | 12.5   | 8.18   |

**Table 5.** Lightning activity in MCS cases, broken down by convective/stratiform regions.

| Date     | Convective CGs |          | Stratiform CGs |          | Convective large iCMCs |          | Stratiform large iCMCs |          | Convective SC iCMCs |          | Stratiform SC iCMCs |          |
|----------|----------------|----------|----------------|----------|------------------------|----------|------------------------|----------|---------------------|----------|---------------------|----------|
|          | Negative       | Positive | Negative       | Positive | Negative               | Positive | Negative               | Positive | Negative            | Positive | Negative            | Positive |
| 20110616 | 4242           | 6303     | 1493           | 2170     | 42                     | 600      | 38                     | 341      | 0                   | 20       | 5                   | 65       |
| 20110624 | 11120          | 4857     | 2159           | 2007     | 64                     | 525      | 47                     | 321      | 0                   | 37       | 3                   | 80       |
| 20110704 | 6008           | 5955     | 1296           | 1357     | 45                     | 682      | 26                     | 137      | 14                  | 40       | 28                  | 53       |
| 20110818 | 12652          | 6238     | 1633           | 1795     | 61                     | 486      | 43                     | 180      | 1                   | 62       | 6                   | 103      |
| 20120430 | 11256          | 6266     | 5181           | 3042     | 62                     | 455      | 91                     | 194      | 3                   | 62       | 3                   | 65       |
| 20120614 | 19597          | 10093    | 5519           | 6047     | 98                     | 620      | 142                    | 535      | 7                   | 68       | 7                   | 197      |
| 20120615 | 2791           | 2231     | 984            | 1302     | 30                     | 252      | 43                     | 272      | 1                   | 13       | 1                   | 41       |
| 20120705 | 7982           | 3089     | 1519           | 1569     | 62                     | 282      | 25                     | 252      | 1                   | 23       | 1                   | 52       |

**Table 6.** Tabulation of ratios of large iCMCs and sprite-class iCMCs to CGs.

| Date     | Large iCMC/CG ratios |            |             |             | Sprite-Class iCMC/CG ratios |            |             |             |
|----------|----------------------|------------|-------------|-------------|-----------------------------|------------|-------------|-------------|
|          | Neg. Conv.           | Pos. Conv. | Neg. Strat. | Pos. Strat. | Neg. Conv.                  | Pos. Conv. | Neg. Strat. | Pos. Strat. |
| 20110616 | 0.99%                | 9.52%      | 2.55%       | 15.71%      | 0.00%                       | 0.32%      | 0.33%       | 3.00%       |
| 20110624 | 0.58%                | 10.81%     | 2.18%       | 15.99%      | 0.00%                       | 0.76%      | 0.14%       | 3.99%       |
| 20110704 | 0.75%                | 11.45%     | 2.01%       | 10.10%      | 0.23%                       | 0.67%      | 2.16%       | 3.91%       |
| 20110818 | 0.48%                | 7.79%      | 2.63%       | 10.03%      | 0.01%                       | 0.99%      | 0.37%       | 5.74%       |
| 20120430 | 0.55%                | 7.26%      | 1.76%       | 6.38%       | 0.03%                       | 0.99%      | 0.06%       | 2.14%       |
| 20120614 | 0.50%                | 6.14%      | 2.57%       | 8.85%       | 0.04%                       | 0.67%      | 0.13%       | 3.26%       |
| 20120615 | 1.07%                | 11.30%     | 4.37%       | 20.89%      | 0.04%                       | 0.58%      | 0.10%       | 3.15%       |
| 20120705 | 0.78%                | 9.13%      | 1.65%       | 16.06%      | 0.01%                       | 0.74%      | 0.07%       | 3.31%       |

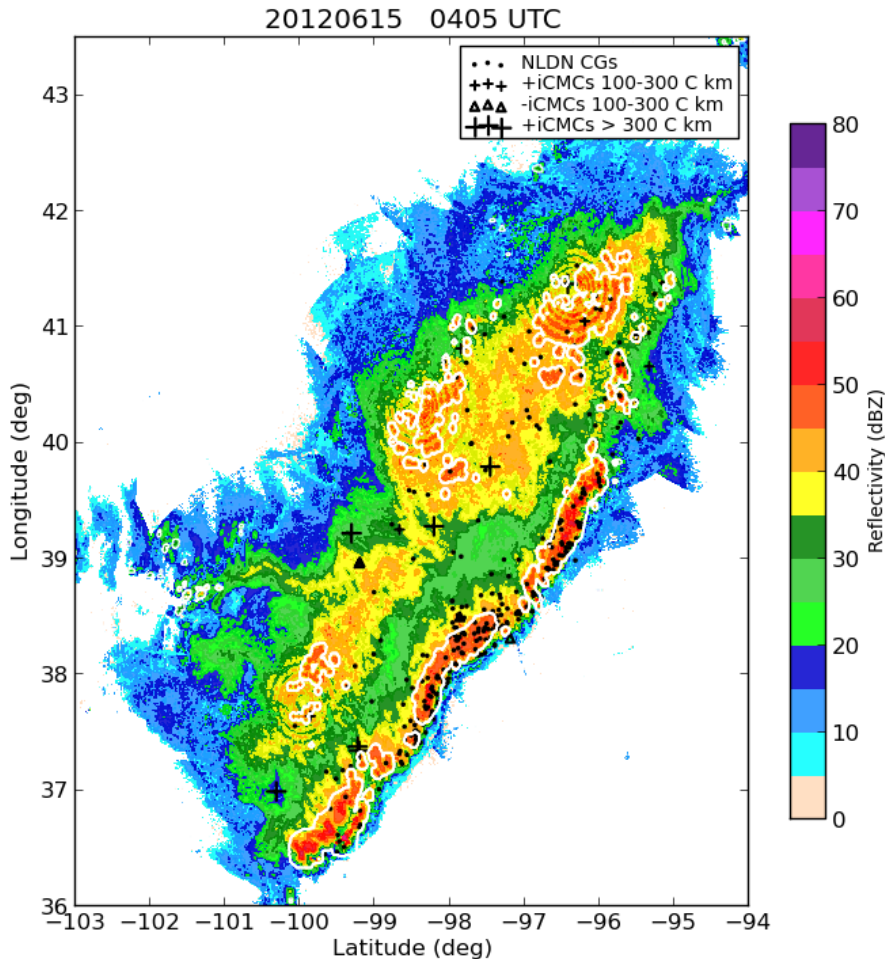


**Figure 10.** Plan view of radar reflectivity at 0405 UTC, 20120615, during the 20120614 MCS. Contoured is reflectivity (dBZ), with white outlined areas being areas of identified convection by the Yuter and Houze (1998) convective/stratiform partitioning method. The black dots represent NLDN CGs. Large black crosses are sprite-class iCMCs, while small crosses are large iCMCs. The small triangles represent negative large iCMCs. No sprite-class negative iCMCs were present in this volume. The values of the six sprite-class +iCMCs in this volume are (in C km), from N to S: 406, 349, 505, 455, 321, 453. The 455 and 321 C km strokes are nearly collocated.

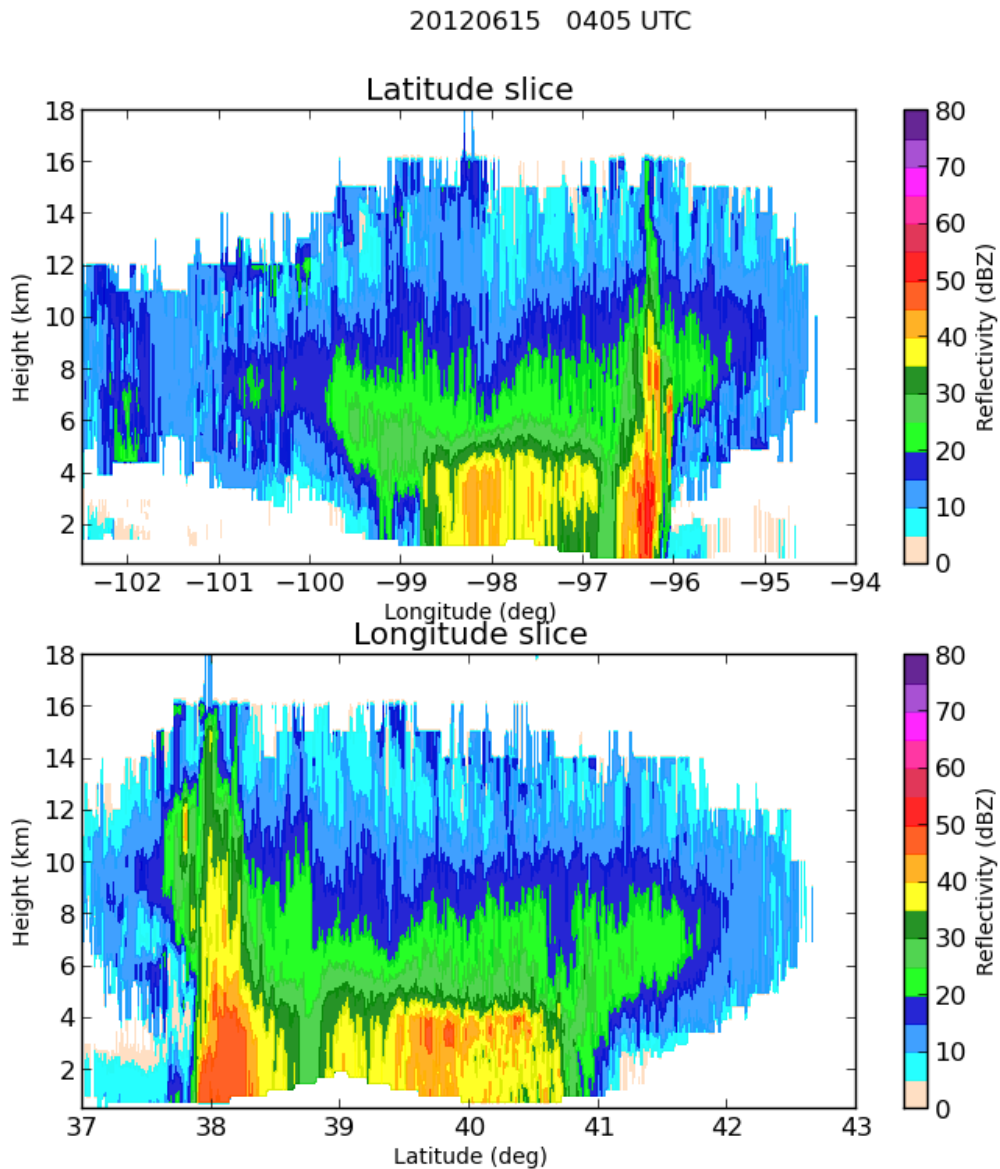


**Figure 11.** Vertical cross section at 0405 UTC, 20120615, during the 20120614 MCS. The top panel is a constant-latitude cross-section through the MCS at approximately  $39.5^{\circ}$  N, nearly coincident with the three sprite-class iCMCs in the stratiform region. The constant-longitude cross-section (bottom panel) is through the center sprite-class iCMC deep in the stratiform, at approximately  $98.5^{\circ}$  W.

### *b. Temporal evolution of variables*

Shown in Figs. 12 and 13 are time series plots from the 20110616 case. The behavior of the variables within the lifecycle of this MCS is similar to the other MCSs. Figs. 14-19 are shown for reference, detailing results of the smallest MCS (20110818), the largest MCS (20120614) and the 20120430 MCS. In Fig. 12a, the iCMC activity per 5 minute volume is plotted against the 1-hour moving average of the stratiform area. It is evident that the peak in large iCMC activity occurs at the time of the most rapid growth of the stratiform area. The peak in sprite-class iCMC activity occurs roughly at the maximum areal coverage of the stratiform area. An offset of approximately 2-3 hours occurs from the start of rapid stratiform growth to the peak sprite-class iCMC activity. Fig. 12b shows the breakdown of large iCMCs and sprite-class iCMCs in the stratiform region, where the notable 2-3 hour delay is evident. As the stratiform area begins to dissipate, all iCMC activity rapidly falls off. Shown in Figs. 12c and 12d are the CG rates plotted against convective and stratiform areas and iCMC activity, respectively. The large iCMC activity closely matches the CG rate, aligning with the maximum growth rate of the stratiform area, while the peak in sprite-class iCMC activity occurs about 2-3 hours later.

Fig. 13a shows the height of the convective (40, 50, and 60 dBZ) echoes per volume. As the large iCMC activity peaks, the echo top heights are maximized, and the heights decrease as the overall large iCMC activity and CG activity (Fig. 13b) diminishes. The sprite-class iCMC activity maximum is aligned with the maximum rate at which the convective heights are decreasing. The stratiform area's growth rate is maximized during the highest echo tops (Fig. 13c), and the heights begin rapidly falling off as the stratiform area reaches its maximum extent. Fig. 13d shows the

convective/stratiform fraction of the total area plotted against large and sprite-class iCMC activity. The convective fraction is enhanced during the peak of large iCMCs, and the stratiform fraction increases during the peak of sprite-class iCMCs. Figs. 14, 16, and 18 are the same plots as in Fig. 12, but detailing results from the 2011818, 20120430, and 20120614 cases, respectively. Figs. 15, 17, and 19 are analogous for Fig. 13, for the 20110818, 20120430, and 20120614 cases, respectively.

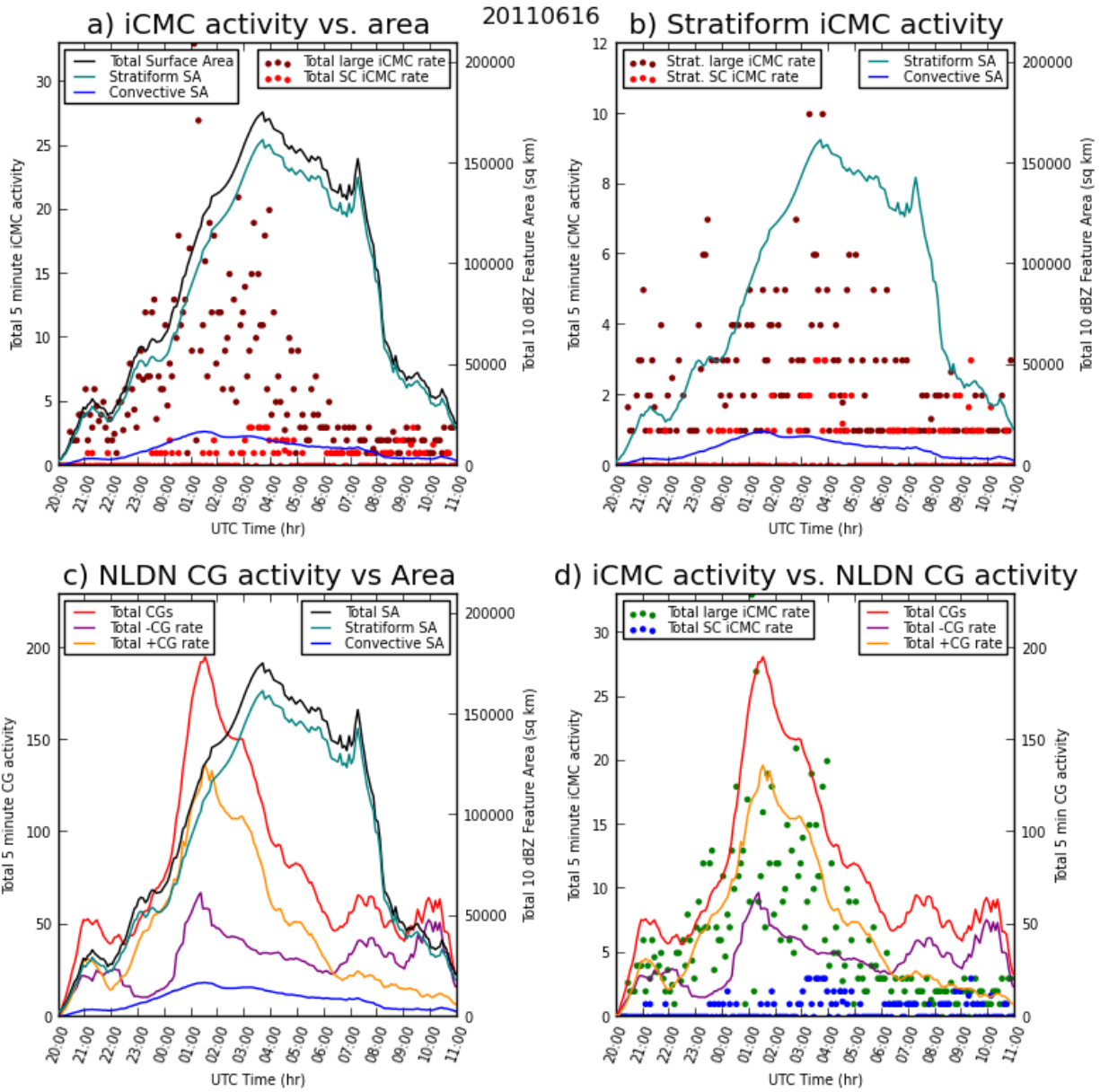


**Figure 12.** Time series representation of variables over the 20110616 MCS lifetime. a) iCMC rate (dots) plotted against 1 hour moving average of feature area. b) Stratiform iCMCs (dots) plotted against 1 hour moving average of feature stratiform area (teal line). c) 1 hour moving average feature areas plotted against 1 hour moving average NLDN CG activity. d) 1 hour moving average CG activity (lines) plotted against iCMC activity (dots)

20110616

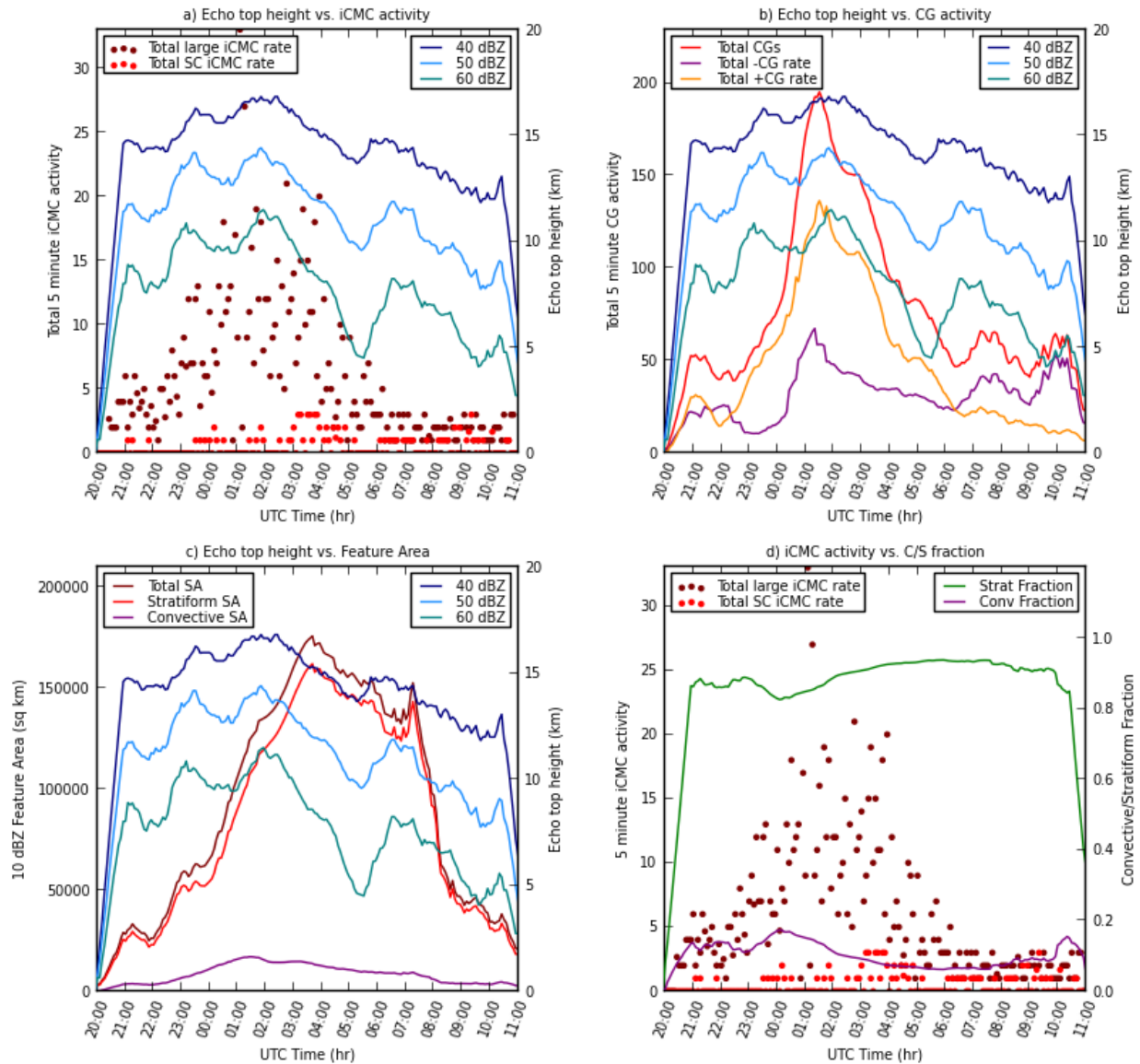


**Figure 13.** Time series representation of convective echo top heights (40,50,60 dBZ) of the 20110616 MCS (1 hour moving average) in km per 5 minute radar volume plotted against: a) 5 minute iCMC activity; b) 1 hour moving average NLDN CG activity; c) 1 hour moving average of 10 dBZ feature convective and stratiform areas; d) convective/stratiform fraction plotted with 5-minute iCMC activity.

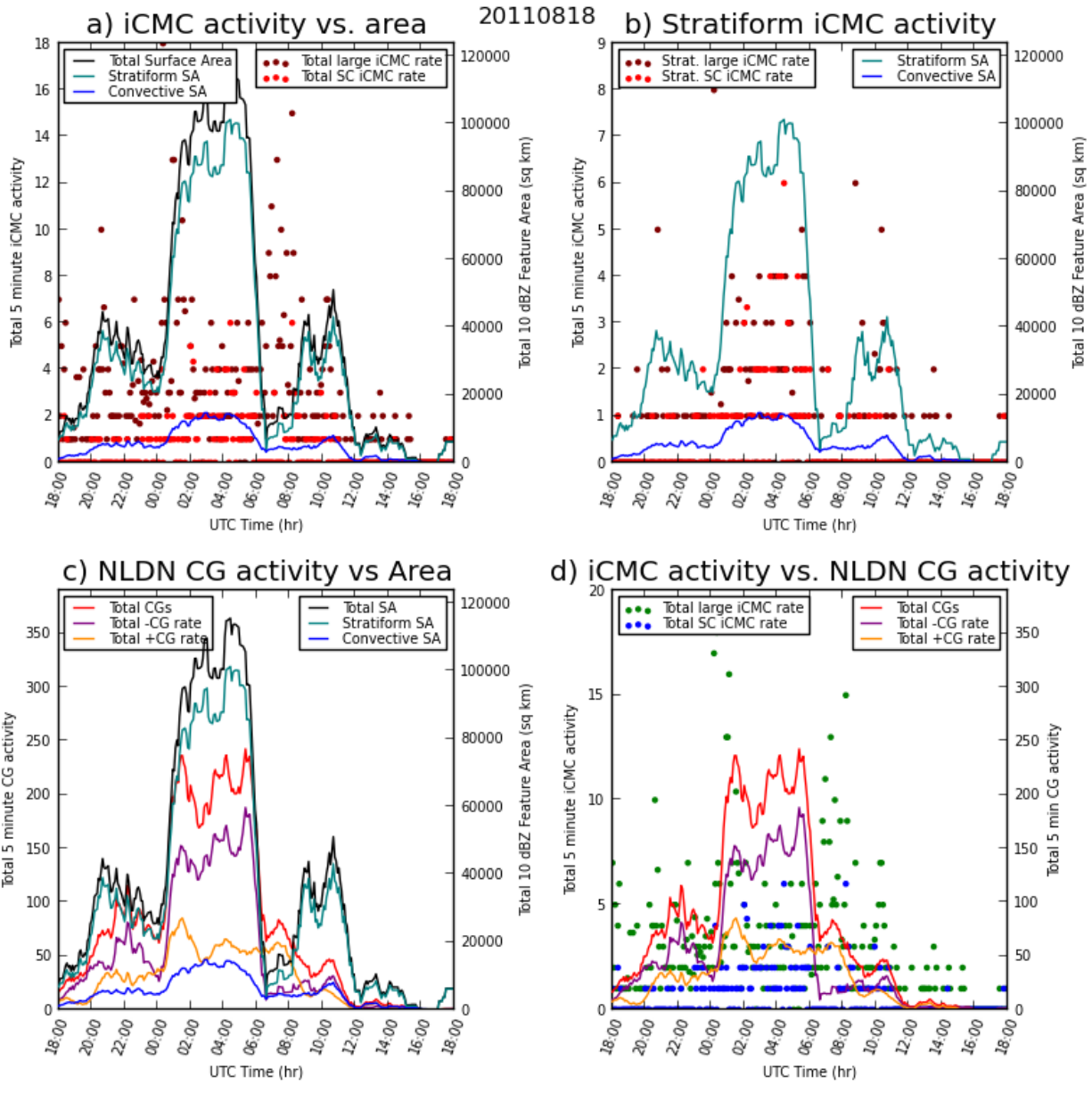


**Figure 14.** Same as in Figure 12, but for the 20110818 MCS.

20110818

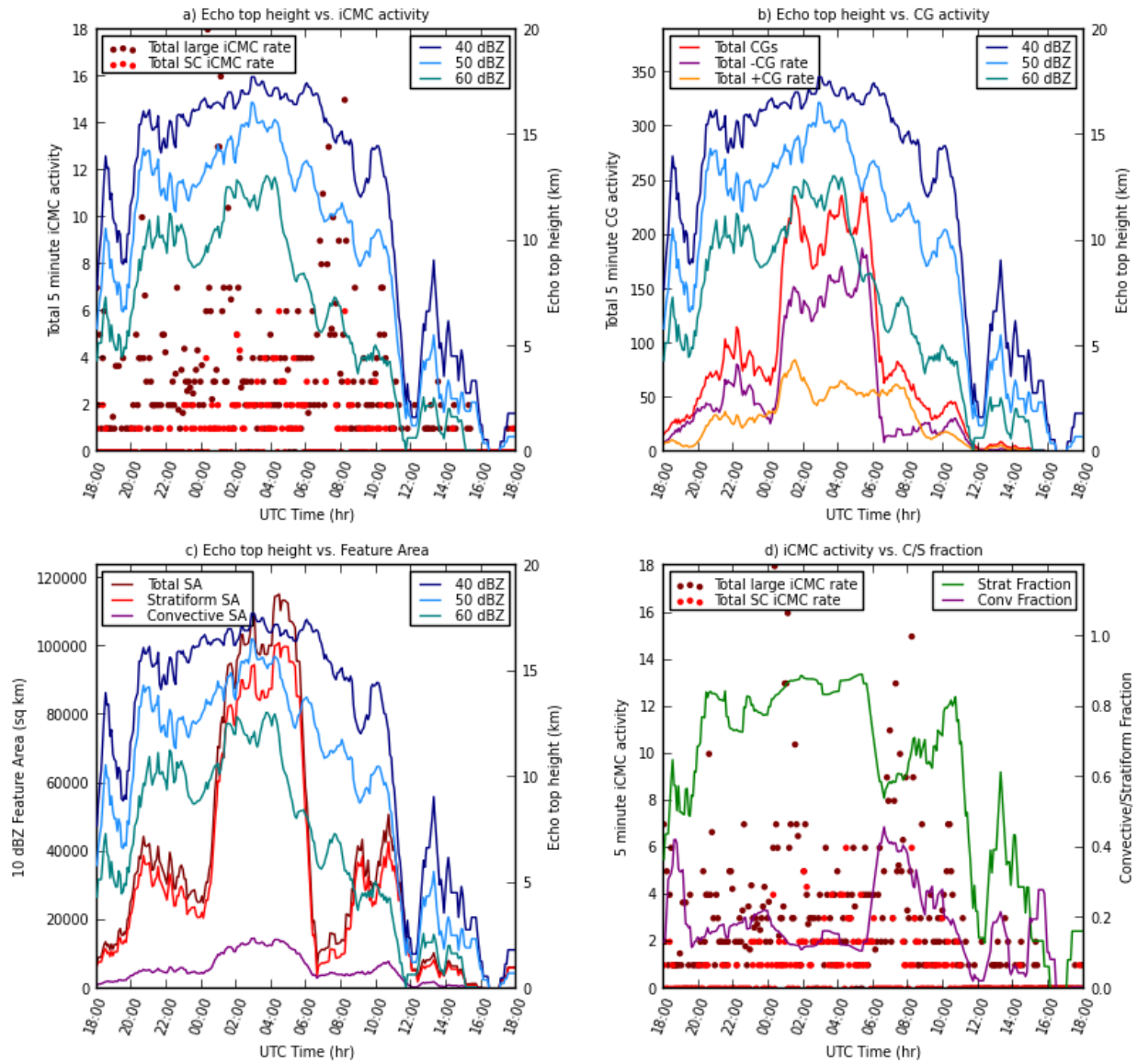


Figure 15. Same as in Figure13, but for the 20110818 MCS.

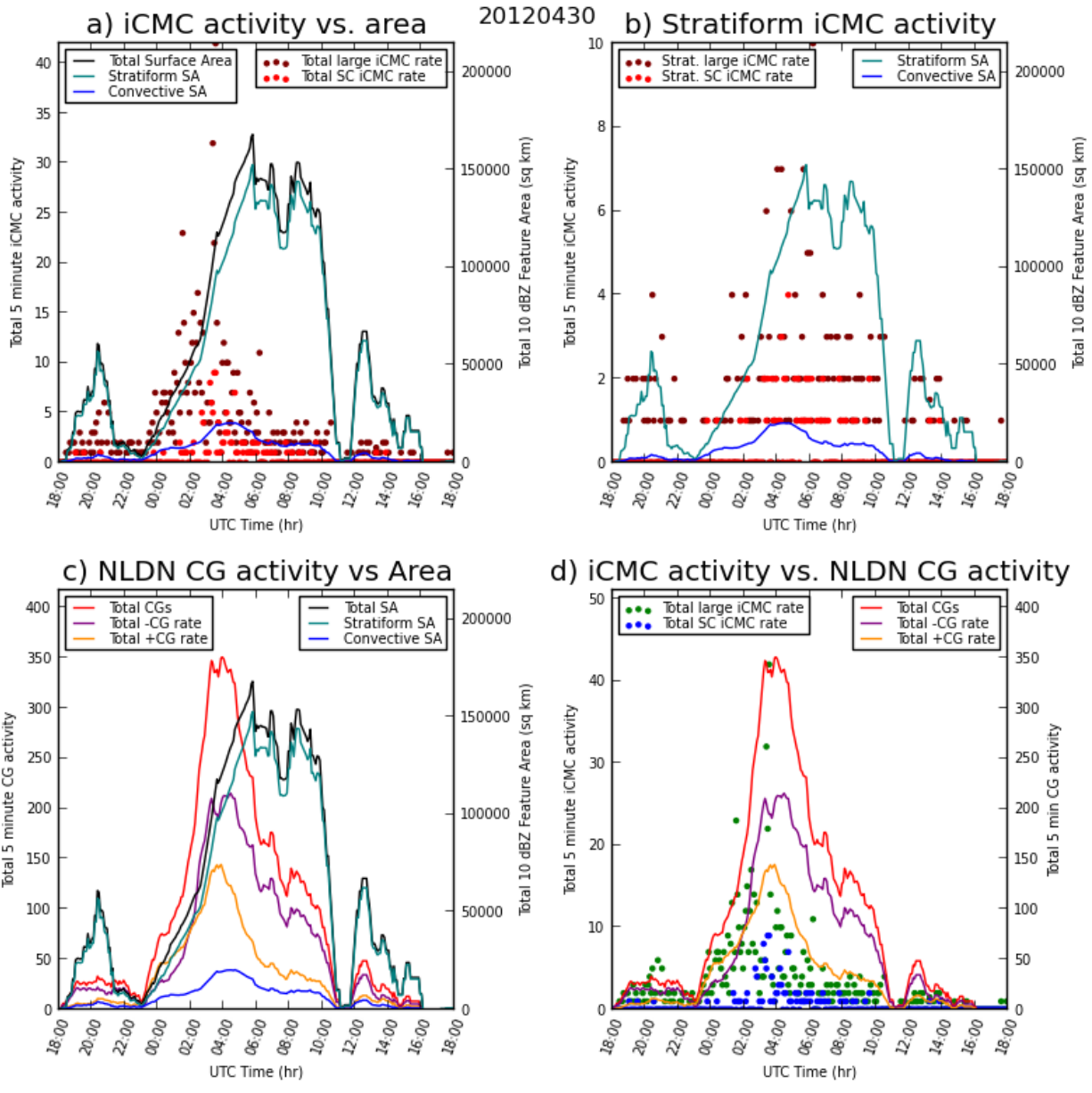


Figure 16. Same as in Figure 12, but for the 20120430 MCS.

20120430

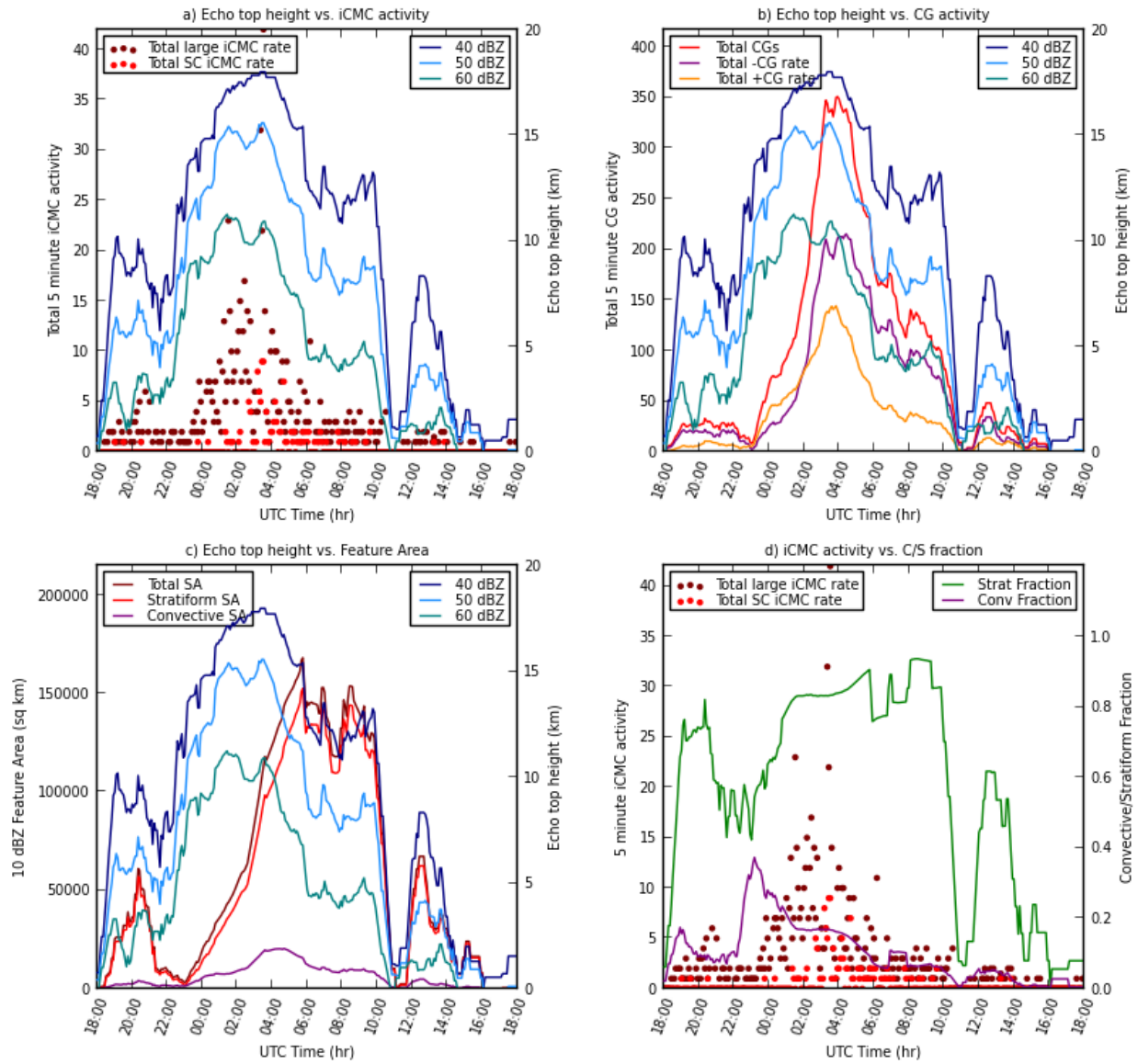


Figure 17. Same as in Figure 13, but for the 20120430 MCS.

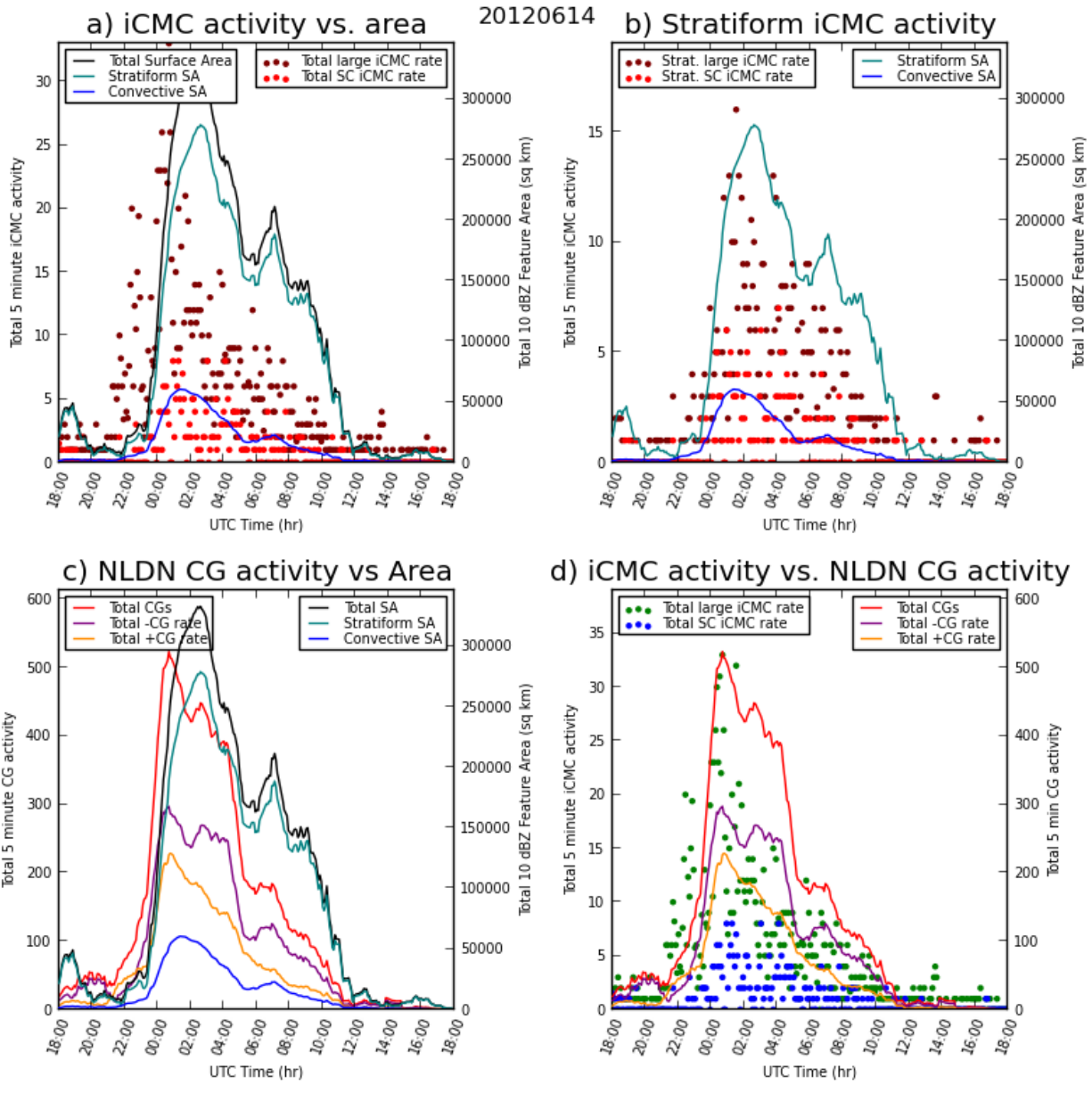


Figure 18. Same as in Figure 12, but for the 20120614 MCS.

20120614

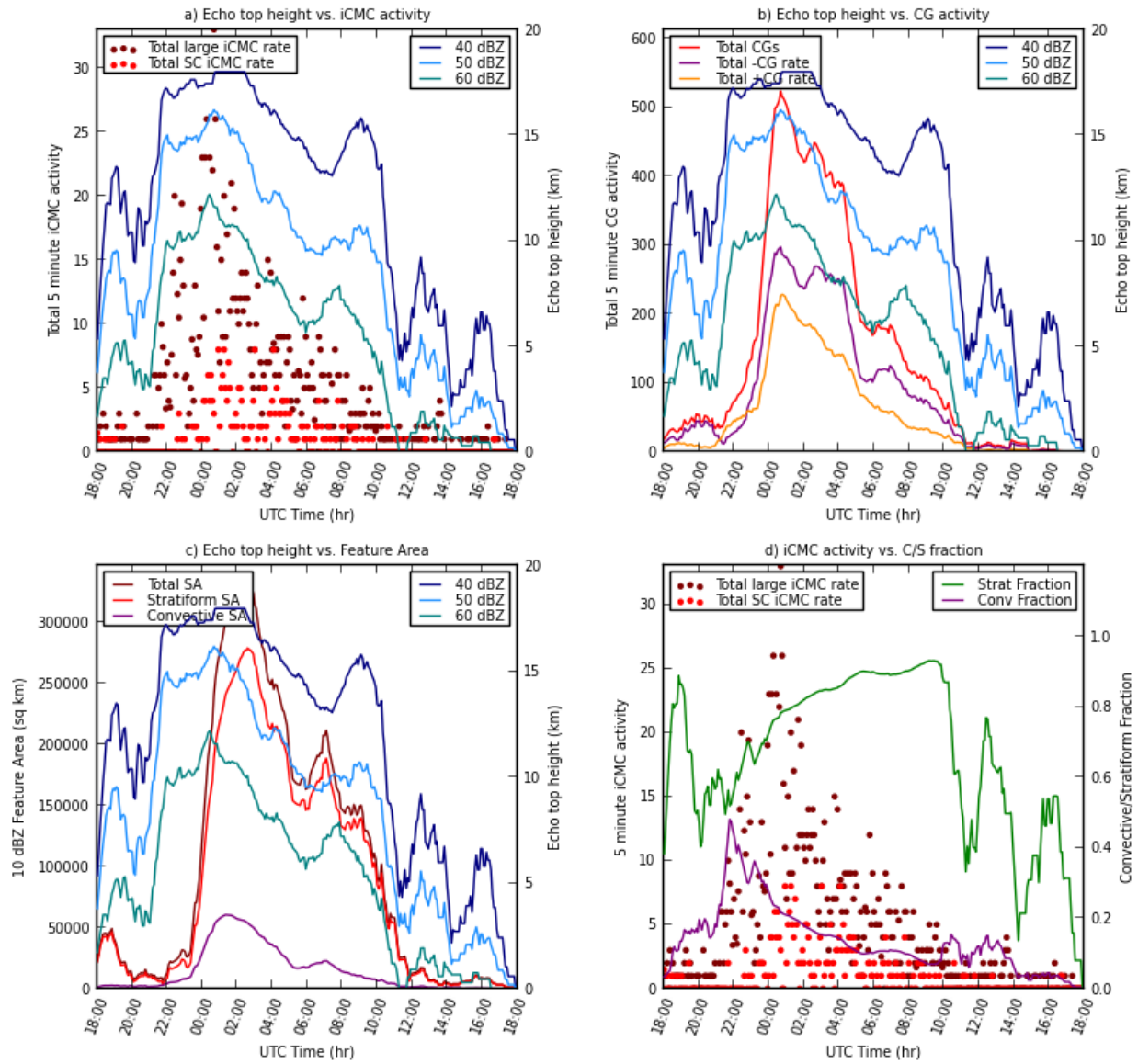


Figure 19. Same as in Figure 13, but for the 20120614 MCS.

## Discussion and Conclusions

Case studies of eight Northern Great Plains warm-season MCSs revealed some fundamental microphysical and statistical characteristics of lightning within MCSs, particularly highly energetic capable of producing sprite-class iCMCs. Analysis of the results presented in the previous chapter is discussed in the following. The results fundamentally follow the findings of Lang et al. (2010b), and build upon the ideas discussed in that study.

As stated previously, the occurrence of sprites above MCSs, particularly associated with large-CMC discharges in the stratiform region of MCSs, is well-known (Boccippio et al. 1995, Williams 1998, Huang et al. 1999, Marshall et al. 2001, Hu et al. 2002, Lyons et al. 2003, 2009, Lang et al. 2010b, 2011a). This study confirms these observations, with a vast majority of sprite-class iCMCs occurring in the stratiform-identified region of MCSs (Table 4; Fig. 14). Also noted was the lag in the peak of sprite-class positive iCMC activity by about 2-3 hours after the onset of rapid stratiform areal growth. This result is clearly linked to the development of the stratiform positive charge reservoir. Lyons et al. (2006) first noted a delay on the order of a couple of hours after storm initiation for sprite (TLE) production, during the mature stage. This study's findings support this hypothesis, on the premise that most sprite-class iCMCs occur during the MCS's mature stage after rapid stratiform growth. This finding is also consistent with the spatial displacement of the maximum of sprite-class iCMCs in the Northern Great Plains eastward of the large iCMC maximum (Cummer et al. 2013, Section 1), in which the lag by 2-3 hours of maximum sprite-class activity can be attributed to the blossoming of the stratiform shield as the MCS propagates to the east.

It can also be noted that as the maximum heights of convective echoes falls, the overall large iCMC activity in the MCS begins to fall off, and the stratiform sprite-class iCMC activity begins to ramp up. Lyons et al. (2006) presented the observation that sprites “turn off” often within an hour of the 55 dBZ echo disappearing. However, the 55 dBZ echo was not monitored in this study, and the results suggest that as convection begins to weaken, stratiform sprite-class iCMCs begin to ramp up, presumably due to the arrival of advected charge from the convective line (i.e. Rutledge and MacGorman 1988, Rutledge et al 1990). This is also consistent with prevailing warm-season MCS sprite initiation theory (Williams 1998, Lyons et al. 2003, Williams and Yair 2006). Sprite-class iCMCs then continue at elevated rates relative to the rapid stratiform development stage until the MCS begins to dissipate. Unfortunately, sprite-class iCMCs do not guarantee a sprite; they only present a good (75-80%) likelihood of sprite initiation (Cummer and Lyons 2005, Lyons et al. 2009), and cannot provide a direct comparison to observations by Lyons (2006) and Lang et al. (2010b). To confirm, visual evidence of sprites over these MCSs would have to be cross-referenced to sprite-class iCMC strokes.

Some additional observations, including the higher rate found in each MCS of stratiform large and sprite-class iCMC per stratiform CG than convective counterparts is notable. This suggests that a larger portion of strokes of both polarities in the stratiform regions of MCSs are more energetic (higher peak current) or have longer continuing currents than in convective areas, broadly consistent for positives with Lyons et al. (1998). However, extensive studies of negative stratiform flashes in MCSs have not been conducted, and the hypothesis presented here should be verified with future studies. The higher fraction of positive strokes to produced large or sprite-class iCMCs

in High Plains MCSs supports previous observations that positive strokes are more likely to have higher peak currents (Lyons et al. 1998) or longer continuing currents (Lyons et al. 2003). The stratiform large positive iCMC fraction varied more (from 6-20% of stratiform +CGs) than sprite-class +iCMCs (from 2-5%), and coupled with the close behavior of large iCMCs to CGs, this suggests that sprite-class iCMC strokes have fundamentally different behavior than large iCMC strokes. It is possible that large iCMC strokes have less robust continuing currents than sprite-class iCMC strokes, which can be amplified by the presence of expansive charge reservoirs, as this study suggests. This is similar to recent work by Chronis et al. (2013, submitted), in which the authors present observations of low flash rates allowing buildup of charge that can be neutralized by a single subsequent stroke, with high peak current and a high iCMC/CMC. The decrease in flash rates (CG activity) seen as the sprite-class iCMC production increases in the MCSs in this study supports the occurrence of this mechanism. More research into why an MCS produces more or less energetic lightning (higher fraction of large and sprite-class iCMCs to CGs) may yield some valuable results, especially to aviation and electrical engineering applications.

To get at the areal coverage utilized by a sprite-class iCMC, a simple calculation can be invoked. Using the estimation of approximately  $150 \text{ km}^3$  for a TLE discharge volume (Lang et al 2011a), and a positive charge layer depth of 0.5 km for a positive charge layer at  $z = 4 \text{ km}$  in the Type B charge structure (Marshall and Rust 1993), it can be surmised that approximately  $300 \text{ km}^2$  of the stratiform charge layer per sprite-class iCMC is being tapped. In the 0405 UTC volume shown in Fig. 2, there are 6 sprite-class positive iCMCs located in the stratiform region, so approximately  $1,800 \text{ km}^2$  of the approximately  $210,000 \text{ km}^2$  (approx. 8.5%) could be assumed to be tapped in that 5

minute volume by the sprite-class iCMCs. However, some of the sprite-class iCMCs were located within 20 km of the convective line, and may not have utilized as much of the stratiform reservoir as those located far within the stratiform region. For an estimate of charge, the iCMC values in Fig. 10 are used, and assuming that the 4 km height was the path length to ground of each of the parent CGs (not the best assumption, as there are likely multiple positive charge layers; Marshall and Rust 1993, Stolzenburg et al. 1994, Lang et al. 2010b) an approximate value of  $3.0 \times 10^6$  C of charge was neutralized within this particular 5-minute volume by the 4 km charge layer over the duration of the iCMC in each case. This value is an underestimate of the total charge, because there were likely longer continuing currents associated with these +CGs (Reising et al. 1996, Bell et al. 1998, Lyons et al. 2003), and iCMC is less than the total CMC (Lyons et al. 2003, Lyons and Cummer 2008). Using this value of charge would require that the 4 km positive charge layer have a charge density of roughly  $28 \text{ nC m}^{-3}$ , which is approximately a factor of two larger than modeled values of  $15 \text{ nC m}^{-3}$  (accounting for both in situ and advective charge densities, from Schuur and Rutledge 2000b), and isn't entirely unreasonable. It also suggests that the charge neutralized within a single radar volume can be significant, and that the processes to replenish this charge are significant contributors on sub-storm timescales to the production of sprite-class iCMCs.

As has been the case in the past, a definitive single charging mechanism for discharges within the stratiform region of an MCS has been difficult to pinpoint. One such mechanism supports charge advection on ice particles ejected aloft from convective cores and advected by storm-relative mesoscale flow into the stratiform region (Smull and Houze 1985; Rutledge and Houze 1987, Rutledge and MacGorman 1988). However, *in situ* charging within the mesoscale updraft (via non-inductive

charging; Takahashi 1978) within the stratiform region is also a significant contributor to the positive charge reservoir (Rutledge et al. 1990, Rutledge and Petersen 1994, Schuur and Rutledge 2000b). This expansive positive charge reservoir is speculated to be the main source of the charge tapped by large and sprite-class positive iCMCs in the stratiform regions of the MCS (Section 1). Noting that more intense convection produced more overall iCMCs within the stratiform region, it can be speculated that enhanced convection in an MCS is responsible for higher rates of sprite-class iCMC production. The increase in available charge would likely come in the form of enhanced charge advection into the stratiform region from the convective line (MacGorman and Rutledge 1988, Rutledge et al. 1990), but also as enhanced *in situ* charging from a potentially stronger mesoscale updraft due to stronger convection (Fritsch and Chappell 1980, Houze 1989), and the relative contributions of each are impossible to determine with the data used in this study.

Lang et al. (2004, 2008) found that many, if not most +CGs their case studies of MCSs come to ground within or very near convective areas while still tapping the positive charge reservoir, and Lang et al. (2010b) found that many sprite +CG parents originated in or near convection, despite coming to ground well outside areas of convection. Looking at a sample 5-minute reflectivity volume for the 20120614 MCS (Fig. 10), this mechanism is qualitatively supported, with sprite-class iCMCs were located both deep within the brightband portion of the stratiform precipitation and very near to convective cores. This also suggests that +CGs tapping different charge layers are possible, and that the existence of multiple positive charge layers may be needed for very high 5 minute sprite-class iCMC rates (as in Fig. 2). However, the location of sprite-class iCMCs well into the stratiform (upwards of 100 km outside the convective

line) indicates that either the flash had a very long path length within the sloping charge layer associated with advection from the convective cores or that the flash was initiated in the stratiform region and had little influence from sources near convection at initiation, instead relying more on charge generated *in situ*. Both processes are likely contributors on a per-flash basis for sprite-class iCMCs deep within stratiform regions. Lightning mapping array (LMA) data (as in Lang et al. 2010b) or direct sounding observations (as in Marshall et al. 1996) are needed to ascertain the locations of charge layer locations.

While *in situ* charging does indeed contribute appreciable charge to the stratiform positive charge reservoir near 0°C (40-70%; Schuur and Rutledge 2000b), it may simply contribute an amount of charge that is scaled by the stratiform area, or the strength of mesoscale ascent (Rutledge and Petersen 1994). A mechanism to explain this is that the *in situ* charging forms a background charge (from which sprite-class iCMCs are certainly possible) but the addition of advected charge from the convective line makes sprite-class iCMC production more favorable (extending Lang et al. 2010b). Illustrating this are comparisons of the 20110616 and 20110624 MCSs with the 20120615 and 20120705 MCSs (Table 6). All four of the MCSs had similar maximum extents to their stratiform areas (Table 4), but the 2011 MCSs contained more vigorous convection than their 2012 counterparts, and produced more sprite-class iCMCs in stratiform regions (as well as overall large iCMCs; Table 6), which can be speculated being caused by the charge advection mechanism. Supporting this speculation is the collocation of sprite-class iCMCs with the falling of maximum convective heights (Figs. 13, 15, 17, and 19), which generally occurs 2-3 hours after the convective height maximum. This 2-3 hour delay broadly matches the charge advection rate from convection hypothesized by Rutledge and MacGorman (1988) and Schuur and Rutledge (2000b).

However, what remains to be explained is how much charge is advected from the convective line, and the timescale at which it occurs in relation to the production of sprite-class iCMCs in stratiform regions. A simple proxy for how much charge is produced stems from Williams (1985), which found that a thunderstorm's electrical activity scales with the size of the storm, as well as the updraft (Petersen et al. 2005a, Deierling et al 2008, Deierling and Petersen 2008). Lang and Rutledge (2002) and Wiens et al. (2005) also found that a larger updraft volume produced more +CGs in High Plains storms. As seen in Table 2, the maximum area of convective activity did not necessarily guarantee more large and sprite-class iCMCs in stratiform areas (not considering the 20120614 case). The total charge produced may be related to findings of total precipitation ice flux correlating linearly with lightning activity (Petersen et al. 2005a, Deierling et al. 2008). Thus, if stronger convection fluxes more ice into upper levels, it is reasonable to conclude that more (positive) charge can be carried on those particles rearward by the storm-relative flow towards the stratiform region. The maximum CG rate in each MCS (Table 4) loosely correlates with increased sprite-class iCMC activity, further suggesting that the vigor of convection is an important factor in advecting charge to the stratiform charge reservoir. However, more than a handful of MCSs would need to be analyzed to confirm this.

These hypotheses and findings offer an insight into the charge structure of MCSs and the relative contributions of charge advection and *in situ* charging towards the production of sprite-class iCMCs. Some of the results and hypotheses presented here need refinement and further testing, and an even larger dataset would help tie down these ideas. Not tested were cold-season MCSs and frontal systems that are capable of producing an iCMC; insight into those systems could provide insight into behavior of

stratiform charge regions in general. In addition, the morphology of an MCS (Parker and Johnson 2000) could also have an impact on the production of sprite-class iCMCs. Additionally, the location of charge layers within an MCS (Marshall and Rust 1993, Lang et al. 2010b, 2011a) could have an influence on the production or magnitude of sprite-class iCMCs, but a fortuitous combination of many MCSs over a long time period over a LMA is likely needed for ascertaining mean charge layer locations.

## Section 2 References

- Bell, T.F., S.C. Reising, and U.S. Inan, 1998: Intense continuing currents following positive cloud-to-ground lightning associated with red sprites. *Geophys. Res. Lett.*, **25**(8), 1285-1288.
- Boccippio, D.J., E.R. Williams, S.J. Heckman, W.A. Lyons, I.T. Baker, and R. Boldi, 1995: Sprites, ELF transients, and positive ground strokes. *Science*, **269**(5227), 1088-1091.
- Carey, L.D., T.L. McCormick, M.J. Murphy, and N.W.S. Demetriades, 2003: Three-Dimensional Radar and Total Lightning Structure of Mesoscale Convective Systems. *Preprints, 31<sup>st</sup> Conf. on Radar Meteorol. Amer. Meteorol. Soc.*, Seattle, WA, pp. 80-83.
- Carey, L. D., M. J. Murphy, T. L. McCormick, and N. W. S. Demetriades, 2005: Lightning location relative to storm structure in a leading-line, trailing-stratiform mesoscale convective system. *J. Geophys. Res.*, **110**, D03105, doi:10.1029/2003JD004371.
- Chronis, T., R. Said, W. Koshak, E. Williams, E. Grant, E. McCaul, and K. Cummins, 2013: New Evidence on the Diurnal Variability of Peak Current in Global CG Lightning, *Bull. Amer. Meteor. Soc.*, submitted.
- Cummer, S. A. and U.S. Inan, 2000: Modeling ELF radio atmospheric propagation and extracting lightning currents from ELF observations. *Radio Science*, **35**(2), 385-394.
- Cummer, S.A., and W.A. Lyons, 2005: Implications of lightning charge moment changes for sprite initiation. *J. Geophys. Res.*, **110**(A04304), doi:10.1029/2004JA010812.

- Cummer, S.A., W.A. Lyons, and M.A. Stanley, 2013: Three Years of Lightning Impulse Charge Moment Change Measurements in the United States. *J. Geophys. Res.*, **118**, 5176-5189, doi:10.1002/jgrd.50442.
- Deierling, W., and W.A. Petersen, 2008: Total lightning activity as an indicator of updraft characteristics. *J. Geophys. Res.*, **113**(D16210), doi:10.1029/2007JD009598.
- Deierling, W., W.A. Petersen, J. Latham, S. Ellis, and H.J. Christian, 2008: The relationship between lightning activity and ice fluxes in thunderstorms. *J. Geophys. Res.*, **113**(D15210), doi:10.1029/2007JD009700.
- Franz, R.C., R.J. Nemzek, and J.R. Winckler, 1990: Television image of a large upward electrical discharge above a thunderstorm system. *Science*, **249**(4964), 48-51.
- Fritsch, J.M., and C.F. Chappell, 1980: Numerical Prediction of Convectively Driven Mesoscale Pressure Systems Part II: Mesoscale Model. *J. Atmos. Sci.*, **37**, 1734-1762.
- Fritsch, J.M., R.J. Kane, and C.R. Chelius, 1986: The Contribution of Mesoscale Convective Weather Systems to the Warm-Season Precipitation in the United States. *J. Climate & App. Met.*, **25**(10), 1333-1345.
- Goodman, S. J., D. R. MacGorman, 1986: Cloud-to-Ground Lightning Activity in Mesoscale Convective Complexes. *Mon. Wea. Rev.*, **114**, 2320-2328.
- Guy, N., X. Zeng, S.A. Rutledge, and W. Tao, 2013: Comparing the Convective Structure and Microphysics in Two Sahelian Mesoscale Convective Systems: Radar Observations and CRM Simulations. *Mon. Wea. Rev.*, **141**, 582-601.
- Houze, R.A. Jr., 1989: Observed Structure of Mesoscale Convective Systems and Implications for Large-scale heating. *Q. J. Roy. Meteor. Soc.*, **115**(487), 425-461.

- Hu, W., S.A. Cummer, W. A. Lyons, and T.E. Nelson, 2002: Lightning charge moment changes for the initiation of sprites. *Geophys. Res. Lett.*, **29**(8), 1279, doi:10.1029/2001GL014593.
- Huang, E., E. Williams, R. Boldi, S. Heckman, W. Lyons, M. Taylor, T. Nelson, and C. Wong, 1999: Criteria for sprites and elves based on Schumann resonance observations. *J. Geophys. Res.*, **104**(D14), 16943-16964.
- Lang, T.J. and S.A. Rutledge, 2002: Relationships between Convective Storm Kinematics, Precipitation, and Lightning. *Mon. Wea. Rev.*, **130**, 2492-2506.
- Lang, T.J., S.A. Rutledge, and K.C. Wiens, 2004: Origins of positive cloud-to-ground lightning flashes in the stratiform region of a mesoscale convective system. *Geophys. Res. Lett.*, **31**(L10105), doi:10.1029/2004GL019823.
- Lang, T.J., D.A. Ahijevych, S.W. Nesbitt, R.E. Carbone, S.A. Rutledge, and R. Cifelli, 2007: Radar-observed Characteristics of Precipitating Systems during NAME 2004. *J. Climate*, **20**, 1713-1733.
- Lang, T. J., and S. A. Rutledge, 2008: Kinematic, microphysical, and electrical aspects of an asymmetric bow-echo mesoscale convective system observed during STEPS 2000. *J. Geophys. Res.*, **113**, D08213, doi:10.1029/2006JD007709.
- Lang, T. J., W. A. Lyons, S. A. Rutledge, J. Meyer, D. R. MacGorman, and S. A. Cummer, 2010b: Transient luminous events above two mesoscale convective systems: Storm structure and evolution. *J. Geophys. Res.*, **115**, A00E22, doi:10.1029/2009JA014500.
- Lang, T. J., J. Li, W. A. Lyons, S. A. Cummer, S. A. Rutledge, and D. R. MacGorman, 2011a: Transient luminous events above two mesoscale convective systems:

- Charge moment change analysis. *J. Geophys. Res.*, **116**, A10306, doi:10.1029/2011JA016758.
- Lang, T. J., S. A. Cummer, S. A. Rutledge, and W. A. Lyons, 2013: The meteorology of negative cloud-to-ground lightning strokes with large charge moment changes: Implications for negative sprites. Accepted in *J. Geophys. Res. Atmos.*
- Lyons, W. A., 1996: Sprite observations above the U.S. High Plains in relation to their parent thunderstorm systems. *J. Geophys. Res.*, **101**, 29,641-29,652.
- Lyons, W.A., M. Uliasz, and T.E. Nelson, 1998: Large Peak Current Cloud-to-Ground Lightning Flashes during the Summer Months in the Contiguous United States. *Mon. Wea. Rev.*, **126**, 2217-2233.
- Lyons, W. A., T. E. Nelson, E. R. Williams, S. A. Cummer, and M. A. Stanley, 2003: Characteristics of sprite-producing positive cloud-to-ground lightning during the 19 July 2000 STEPS mesoscale convective systems. *Mon. Wea. Rev.*, **131**, 2417-2427.
- Lyons, W.A., 2006: The Meteorology of Transient Luminous Events- An Introduction and Overview, Chapter 1, NATO Advanced Study Institute, Sprites, Elves, and Intense Lightning Discharges, NATO Science Series II (Mathematics, Physics, and Chemistry), **225**, Springer Publishing House, M. Fullekrug, Ed., Conte, Corsica, 19-56.
- Lyons, W.A., L.M. Andersen, T.E. Nelson, and G.R. Huffines, 2006: Characteristics of sprite-producing electrical storms in the STEPS 2000 domain. On line summary and CD, 2<sup>nd</sup> Conf. on Meteorological Applications of Lightning Data, AMS, Atlanta, 19 pp.

- Lyons, W.A. and S.A. Cummer, 2008: Stratospheric Lightning: Forecasting and Nowcasting Tools. Final Report, SBIR Phase II, Missile Defense Agency, Contract HQ0006-06-C-7313, FMA Research, Inc., Fort Collins, CO, 298 pp.
- Lyons, W. A., M. Stanley, J. D. Meyer, T. E. Nelson, S. A. Rutledge, T. J. Lang, and S. A. Cummer, 2009: The meteorological and electrical structure of TLE-producing convective storms. In *Lightning: Principles, Instruments and Applications*, H.D. Betz et al. (eds.), 389-417 pp., Springer Science+Business Media B.V., DOI: 10.1007/978-1-4020-9079-0\_17.
- Maddox, R. A., 1980: Mesoscale Convective Complexes. *Bull. Amer. Meteor. Soc.*, **61**, 1374-1387.
- Makowski, J. A., D. R. MacGorman, M. I. Biggerstaff, and W. H. Beasley, 2013: Total Lightning Characteristics Relative to Radar and Satellite Observations of Oklahoma Mesoscale Convective Systems. *Mon. Wea. Rev.*, **141**, 1593-1611.
- Mapes, B.E., 1993: Gregarious Tropical Convection. *J. Atmos. Sci.*, **50**(13), 2026-2037.
- Marshall, T.C. and W.D. Rust, 1993: Two types of vertical electrical structure in stratiform precipitation systems of mesoscale convective systems. *Bull. Amer. Meteor. Soc.*, **74**(11), 2159-2170.
- Marshall, T.C., M. Stolzenburg, W.D. Rust, E.R. Williams, and R. Boldi, 2001: Positive charge in the stratiform cloud of a mesoscale convective system. *J. Geophys. Res.*, **106**(D1), 1157-1163.
- Miller, D. and J.M. Fritsch, 1991: Mesoscale Convective Complexes in the Western Pacific Region. *Mon. Wea. Rev.*, **119**, 2978-2992.

- McAnelly, R. L. and W. R. Cotton, 1989: The Precipitation Life Cycle of Mesoscale Convective Complexes over the Central United States. *Mon. Wea. Rev.*, **117**, 784-808.
- Qin, J., S. J. Celestin, and V. P. Pasko, 2012: Minimum charge moment change in positive and negative cloud to ground lightning discharges producing sprites. *Geophys. Res. Lett.*, **39**, L22801, doi:10.1029/2012GL053951.
- Parker, M. D. and R. H. Johnson, 2000: Organizational Modes of Midlatitude Mesoscale Convective Systems. *Mon. Wea. Rev.*, **128**, 3413-3436.
- Pasko, V.P., U.S. Inan, and T.F. Bell, 2001: Mesosphere-troposphere coupling due to sprites, *Geophys. Res. Lett.*, **28**(19), 3821-3824.
- Petersen, W.A., H.J. Christian, and S.A. Rutledge, 2005a: TRMM observations of the global relationship between ice water content and lightning. *Geophys. Res. Lett.*, **32**(L14819), doi:10.1029/2005GL023236.
- Rakov, V.A. and M. A. Uman, 2003: *Lightning*. Cambridge University Press, Cambridge, 687 pp.
- Reising, S.C., U.S. Inan, T.F. Bell, and W.A. Lyons, 1996: Evidence for continuing currents in sprite-producing cloud-to-ground lightning. *Geophys. Res. Lett.*, **23**(24), 3639-3642.
- Rutledge, S.A., and R.A. Houze, Jr., 1987: A Diagnostic Modeling Study of the Trailing Stratiform Region of a Midlatitude Squall Line, *J. Atmos. Sci.*, **44**(18), 2640-2656.
- Rutledge, S.A., and D. R. MacGorman, 1988: Cloud-to-ground Lightning Activity in the 10-11 June 1985 Mesoscale Convective System Observed during the Oklahoma-Kansas PRE-STORM Project. *Mon. Wea. Rev.*, **116**, 1393-1408.

- Rutledge, S. A., R.A. Houze, Jr., M.I. Biggerstaff, and T. Matejka, 1988: The Oklahoma-Kansas Mesoscale Convective System of 10-11 June 1985: Precipitation Structure and Single-Doppler Radar Analysis. *Mon. Wea. Rev.*, **116**, 1409-1430.
- Rutledge, S.A., C. Lu, and D.R. MacGorman, 1990: Positive Cloud-to-Ground Lightning in Mesoscale Convective Systems. *J. Atmos. Sci.*, **47**(17), 2085-2100.
- Rutledge, S.A., and W.A. Petersen, 1994: Vertical radar reflectivity structure and cloud-to-ground lightning in the stratiform region of MCSs: Further evidence for in-situ charging in the stratiform region. *Mon. Wea. Rev.*, **122**, 1760-1776.
- Schuur, T.J., and S.A. Rutledge, 2000b: Electrification of Stratiform Regions in Mesoscale Convective Systems. Part II: Two-Dimensional Numerical Model Simulations of a Symmetric MCS. *J. Atmos. Sci.*, **57**, 1983-2006.
- Shepherd, T.R., W. D. Rust, and T.C. Marshall, 1996: Electric Fields and Charges near 0°C in Stratiform Clouds, *Mon. Wea. Rev.*, **124**, 919-938.
- Smull, B.F., and R.A. Houze, Jr. (1985): A Midlatitude Squall Line with a Trailing Region of Stratiform Rain: Radar and Satellite Observations. *Mon. Wea. Rev.*, **113**, 117-133.
- Steiner, M. and J.A. Smith, 2002: Use of Three-Dimensional Reflectivity Structure for Automated Detection and Removal of Nonprecipitating Echoes in Radar Data. *J. Atmos. Ocean Tech.*, **19**, 673-686.
- Stolzenburg, M., T.C. Marshall, W.D. Rust, and B.F. Smull, 1994: Horizontal Distribution of electrical and meteorological conditions across the stratiform region of a mesoscale convective system. *Mon. Wea. Rev.*, **122**, 1777-1797.

- Stolzenburg, M., W.D. Rust, B.F. Smull, and T.C. Marshall, 1998a: Electrical structure in thunderstorm convective regions, 1. Mesoscale convective systems. *J. Geophys. Res.*, **103**(D12), 14059-14078.
- Takahashi, T., 1978: Riming electrification as a charge generation mechanism in thunderstorms. *J. Atmos. Sci.*, **35**, 1536-1548.
- Wiens, K.C., S.A. Rutledge, and S.A. Tessendorf, 2005: The 29 June 2000 supercell observed during STEPS. Part II: Lightning and Charge Structure. *J. Atmos. Sci.*, **62**, 4151-4177.
- Williams, E.R., 1985: Large-scale charge separation in thunderclouds. *J. Geophys. Res.*, **90**, 6013-6025.
- Williams, E.R., 1998: The positive charge reservoir for sprite-producing lightning, *J. Atmos. Solar-Terres. Phys.*, **60**, 689-692.
- Williams, E.R. and Y. Yair, 2006: The microphysical and electrical properties of sprite-producing thunderstorms. NATO Advanced Study Institute on Sprites, Elves and Intense Lightning Discharges, M. Fullekrug et al. (eds.), Springer, 57-83.
- Williams, E., et al., 2012: Resolution of the sprite polarity paradox: The role of halos. *Radio Sci.*, **47**, RS2002, doi:10.1029/2011RS004794.
- Yuter, S. and R. A. Houze Jr. ,1998: The natural variability of precipitating clouds over the western Pacific warm pool, *Q.J.R. Meteorol. Soc.*, **124**, 53-99.
- Zhang, J., C. Langston, and K. Howard, 2008: Brightband Identification Based on Vertical Profiles of Reflectivity from the WSR-88D, *J. Atmos. Ocean. Tech.*, **25**, 1859-1872.

Zhang, J., and Coauthors, 2011: National Mosaic and Multi-Senson QPE (NMQ)

System: Description, Results, and Future Plans, *Bull. Amer. Met. Soc.*, **92**, 1321-1338.

## OVERALL CONCLUSIONS

In Section 1, regional, seasonal, and diurnal observations of large and sprite-class iCMC activity over the contiguous United States are presented.

Strong seasonal and diurnal variations in large and sprite-class iCMC activity were noted in many regions. As the seasons progressed from winter to summer, it was noted that the northwestward march from the Southeastern US to the Central Plains in maxima of both polarities of iCMCs compared well to similar findings in MCSs (Velasco and Fritsch 1987), CGs (Holle et al. 2011), and overall lightning (Christian et al. 2003). Diurnally, the MCS signature is strong in the Northern Great Plains region (supporting Cummer et al. 2013, Section 1), the Gulf Stream was a prolific producer of large iCMCs year round (consistent with Christian et al. 2003, Virts et al. 2013), and the Intermountain West distribution of large iCMCs showed a strong influence of diurnally-forced convection, particularly associated with the North American Monsoon (Adams and Comrie 1997).

Large positive iCMCs peak later than large negative iCMCs, which was attributed to large negatives being primarily associated with convective development (Lang et al. 2013), and large positives being associated with stratiform areas of MCSs (in NGP) or isolated storms with stratified anvils (e.g. MTN) (extending Rutledge and MacGorman 1988, Rutledge et al. 1990, Boccippio et al. 1995, Williams 1998, Lyons et al. 2003, Lang et al. 2010b, 2011a). The diurnal iCMC observations in the oceanic regime over the Gulf Stream were consistent with findings by Liu and Zipser (2008) and Romatschke et al. (2010) of a morning peak in convection over oceans.

As a final observation in Section 1 and transition into Section 2, it was noted that broad maxima in large and sprite-class positive iCMCs were co-located with the approximate maximum occurrence in High Plains MCSs (Maddox 1980, Fritsch et al. 1986, Ashley et al. 2003). Taking into account well-known observations that positive CGs commonly with high peak currents account for the a significant portion of flashes in the stratiform region of MCSs (Orville et al. 1988, Rutledge and MacGorman 1988, Rutledge et al. 1990), it was surmised that the positive iCMC maximum in the Northern Great Plains was due to the presence of warm-season MCSs. Diurnally, this result was confirmed with the observation of a broad peak in large and sprite-class iCMC activity coming well after local sunset, as MCSs in this region tend to be primarily nocturnal (McAnelly and Cotton 1989).

The MCS case studies in Section 2 were selected to correspond to the regional maximum in the Northern Great Plains of large and sprite-class iCMC production from Section 1. Results from Section 2 supported the conclusions of Section 1, with the peak in sprite-class iCMCs coming 2-3 hours later than the peak in large iCMCs, consistent with both the maturation of stratiform charge reservoirs (Boccippio et al. 1995, Williams 1998, Lyons et al. 2003) in a diurnal, storm-lifetime sense and in a regional sense, from the advection of MCSs eastward as they mature (McAnelly and Cotton 1989), consistent with the displacement of the sprite-class +iCMC maximum eastward of the large +iCMC maximum seen in Cummer et al. (2013) and Section 1.

The rapid growth of the stratiform region coincident with the peak in large iCMC activity along with the peak in sprite-class iCMC activity while the stratiform area was maximized strongly supported the hypothesis in Section 1, wherein the maximum in positive large and sprite-class iCMCs was attributed to the maturation of positive charge

layers in the stratiform region of MCSs. Additionally, the vast majority of sprite-class iCMCs were found to be positive and in stratiform-identified regions, which supports the hypothesis in Section 1 and previous studies (Bocippio et al. 1995, Williams 1998, Lyons et al. 2003, Lang et al. 2010b, 2011a) that positive CGs within stratiform regions are likely tapping expansive charge layers to reach large values of charge moment changes.

The area of the stratiform shield was a proposed indicator of the capability of an MCS to produce sprite-class iCMC (Bocippio et al. 1995, Williams 1998, Lyons et al. 2003, Lang et al. 2010b, 2011a), but was weakly correlated. Also notable is the likelihood of prolific sprite-class iCMC production within a five minute radar volume to be the result of CGs tapping multiple stratiform charge layers. Also noted was the tendency of positive strokes to have a larger fraction of more energetic strokes (Bocippio et al. 1995, Lyons et al. 1998) than negatives as well as a larger fraction of stratiform flashes to be more energetic than convective flashes.

A relative enhancement of convective activity, seen in the maximum heights of convective (40 and especially 50 and 60 dBZ) echoes, corresponds to a peak in overall CG activity (consistent with Petersen et al. 2005a, Deierling et al 2008) and overall large iCMC activity. Sprite-class iCMC activity was also observed to increase coincident with a decrease in maximum convective echo heights, which suggest that the overall production of CGs and large iCMCs are more closely tied to the MCS's convective enhancement stage and that CGs with sprite-class iCMCs have different basic behavior than CGs with large iCMCs, in that sprite-class iCMCs are likely to have more robust continuing currents from tapping expansive charge layers in the stratiform regions. A lag in sprite-class iCMC activity to convective enhancement also suggests that charge

advection from convective areas (Rutledge and MacGorman 1988, Rutledge et al. 1990, Schuur and Rutledge 2000b) plays a significant role in providing available charge to the stratiform region. Supporting this are results that higher maximum convective heights in two MCSs corresponded to higher sprite-class iCMC production. However, the relative magnitudes of charge contributed by *in situ* charging (Rutledge and Petersen 1994, Schuur and Rutledge 2000b) to charge advection in MCS stratiform regions cannot be determined with the data utilized in this study.

Note: The references in this section draw from references listed in both Section 1 and Section 2. Please refer to the corresponding References section for citation.